Fertigstellung und Inbetriebnahme eines Versuchstands zur Vermessung experimenteller induktiver Batterieladesysteme

Master Thesis

Humbert Vidal

Matrikelnummer: 1989419

26 September 2016

Betreuer: Dipl.-Ing. Benjamin Klaus

Declaration

I hereby declare that I wrote my Master Thesis on my own and that I have followed the regulations relating to good scientific practice of the Karlsruhe Institute of Technology (KIT) in its latest form. I did not use any unacknowledged sources or means and I marked all references I used literally or by content.

Date: Signature

Contents

Abstract

Within the framework of inductive technology, this master's thesis represents the conclusion of several previous projects that pursuit a common objective, to design and develop an inductive wireless power transfer system based in resonant converters.

Together with the research and development of the previous projects, this thesis describes the last tasks implemented in order to perform the construction and set up of a 44 kVA charger with an efficiency of 90%.

The grid power supply is modulated by means of a power inverter switching at frequencies up to 500 kHz. A method to recognise the ideal switching frequency has been designed and implemented. Two different coil systems have been tested, one with high coupling coefficient and another with good behaviour under deviation conditions. The track tuning consists of two capacitors modules, each connected in series with their respective induction coil. In all tests a DC resistor has been used as a system's load.

List of figures

List of tables

Abbreviations

DC	Direct current
AC	Alternating current
emf	Electromotive force
ϕ	Magnetic flux
t	Time
E	Electric field's intensity
I	Current
B	Magnetic flux density
A	Area
H	Magnetic field's intensity
J_f	Free current density
D	Electric displacement field
S	Area
$I_{f,enc}$	Current through the enclosure
μ_0	Vacuum permeability
r	Position of calculation
M	Mutual inductance
k	coupling coefficient
w	angular frequency
L1	Inductance of the primary
L2	Inductance of the secondary
U	Voltage
R	Resistance
X_L	Inductive reactance
Xc	Capacitive reactance
φ	Power factor
S-S	Series-Series compensation
S-P	Series-Parallel compensation
P-S	Parallel-Series compensation
P-P	Parallel-Parallel compensation
ZVS	Zero voltage switching
ZVC	Zero current switching
PCB	Printed circuit board

IC	Integrated circuit
MOSFET	Metal oxide field effect transistor
U_F	On-state voltage drop
P_{FC}	Conduction losses
T	Period
I_F	Forward current
V_{TO}	Voltage drop in a diode
rt	Diode resistance
I_{Favg}	Average forward current
I_{Frms}	RMS forward current
I_{Fmax}	Maximal forward current
P_{Fs}	Switching losses
Q_{rr}	Recovery energy
U_r	Reverse Voltage
f	Frequency
PWM	Pulse width modulation
ECU	Electronic control unit
LCD	Liquid crystal display
CTC	Clear timer on compare match
ICR1	Timer 1 register for Top value
TCNT1	Timer 1 counter register
OC1A	PWM signal's output
OC1B	PWM signal's output
ADC	Analog to digital converter
CPLD	Complex programmable logic device
NTC	Negative
RMS	Root mean square
pos.	Positive
neg.	Negative
SiC	Silicon carbide
AC1	Alternating current connection 1
AC2	Alternating current connection 2
HV+	Positive direct current connection
HV-	Negative direct current connection

Tvjw	Temperature of the virtual joint
Rvjw-th	Thermal resistance between virtual joint and heat sink
Rth-ha	Thermal resistance between heat sink and air
Ta	Ambient temperature
max.	Maximal value

1. Introduction

Since Nikola Tesla in the earlies 1880s showed the world the possibility of wireless power transfer by means of high frequency electromagnetic waves and resonant systems, humanity has been using its properties in many applications such as telecommunications or medical analysis. Nowadays, we are experiencing full expansion of electrical mobility and more and more industries, administration and society are living out this new concept of culture and just as this technology has been improving and growing so does wireless power transmission.

The need for developing and investigating in power transfer systems lies in the fact that every day a major number of electrical vehicles can be seen in the street. In 2015 only in Germany the electric car sales increased a 45%, the hybrid a 23% and plug-in hybrids a 125%. In other words, 12363 new electric cars and 33600 hybrids were allowed on the road for first time and all this cars have batteries that need to be charged. [1]

A strong reason to develop this kind of technology is the substantial simplicity, from the user's point of view, that it gives to the charging process. Within the use of wireless power transfer there is no need for the driver to interact between the grid and the car and the process can be automatized. Therefore, this method offers a safe robust and practical way to perform the charge and that the driver´s only concern is to activate the charging mode and wait until the process is finished.

Figure 1.1 Application of inductive Technology [2]

In the progress of this Master Thesis, the construction and start-up of an inductive power transfer system will be described. In first place, technological basics and mathematical fundamentals are explained in Chapter 2, giving way to the description of system's design and performed tasks in Chapter 3 and 4. In Chapter 5 experiments, measurements, simulations and obtained results are shown. Subsequently a discussion of the results is given in Chapter 6 and finally, additional information like schematics, PCB designs and simulation models can be found in Chapter 7.

2. Fundamentals

Drawn from the information in [4], [5] and [6], this chapter will introduce the concepts needed to understand inductive power transfer and explain the theory behind it.

2.1. System's overview

The aim of this section is to introduce the system and the different elements that take part in the inductive power transfer.

The main components can be divided in 3 groups, each of them performing essential and specific functions.

- Power supply and signal modulation:
  Consists of the grid connection, a three-phase rectifier, the DC link circuit and the power inverter that generates the high frequency AC signal.

- Resonant circuit:
  Includes the primary and secondary winding as well as the capacitors banks to set up the resonant frequency of the system. This elements are the key of inductive power transfer systems. The operating principles will be described below.

- Secondary rectification, filter and load:
  Transforms the AC signal of the secondary circuit to DC. A filter is used to attenuate current and voltage ripples. The load will absorb or dissipate al power received from the circuit, in the development of this thesis the load used will be a DC resistor.

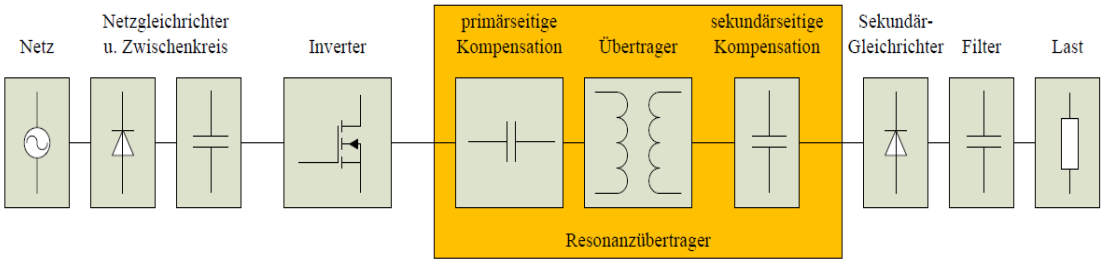

Figure 2.1 System's overview[6]

2.2. The concept of inductive power transfer

The effect of induction and the fundamentals of inductive power transfer are based in two main physical principles. The Faraday's law of induction and the Ampère's law.

The Faraday's law of induction (2.1) states that the voltage induced (emf) in a closed circuit is directly proportional to the variation in time of the magnetic flux linked to this circuit.

$$emf = -\frac{d\phi}{dt} \tag{2.1}$$

The negative sign indicates that the current driven by the induced emf will oppose the change in the magnetic flux.

The integral form of the induction law applying Strokes theorem can be written as shown in the equation (2.2).

$$\oint_C \vec{E} \cdot d\vec{l} = -\frac{d}{dt}\int_S \vec{B} \cdot d\vec{A} \tag{2.2}$$

The Ampère's law (2.3) relates the integrated magnetic field around a closed loop to the electric current passing through the loop. In other words, the relation between a current flowing through a conductor and the generated magnetic field.

$$\oint_C \vec{H} \cdot \vec{dl} = \iint_S \left(\vec{J_f} + \frac{\partial \vec{D}}{\partial t}\right) \cdot \vec{dS} = I_{f,enc} \tag{2.3}$$

This second concept can be also explained applying Biot-Savart law (2.4) which states the same relation between current and magnetic field.

$$B = \frac{I \cdot \mu_0}{4\pi}\oint_C \frac{dl\ x\ \hat{r}}{r^2} \tag{2.4}$$

In a system where current flows through two coils that are closed enough, a mutual magnetic flux is linked to both of them. This part of the magnetic flux that passes through the second surface, S2, can be calculated as can be seen in equation (2.5).

$$\phi_{12} = \int_{S2} B1 \cdot dS \tag{2.5}$$

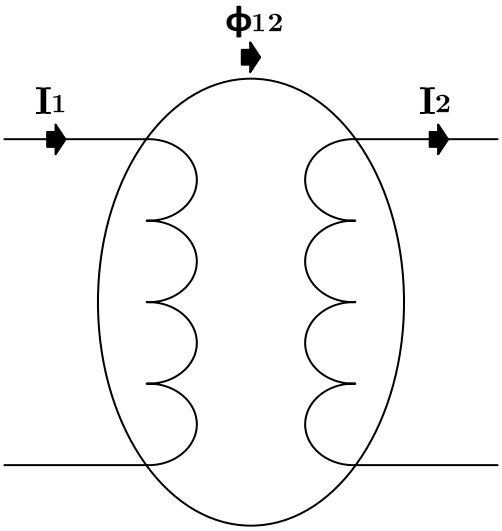

Figure 2.2 Two loops with magnetic coupling and the currents flowing through each loop

The mutual flux ϕ_{12} is proportional to the current I_1. The relation can be written as in equation (2.6).

$$\phi_{12} = M \cdot I_1 \tag{2.6}$$

Where M is the mutual inductance of the coupled loops or inductors.

Expressing L_1 and L_2 as the respective self-inductance for the inductors, an expression of the coupling coefficient (k) can be calculated as shown in equation (2.7).

$$k = \frac{M}{\sqrt{L_1 \cdot L_2}} \tag{2.7}$$

The value of the self-inductance not only depends on the geometry of the loop that determines the inductance, this property is altered by other elements near the inductor, whether ferrite, aluminium plates and the metallic structure of the system itself. In order to contrast and verify the calculations of the coupling coefficient several measures of the self-inductances and the mutual inductance has been performed. Results can be seen in Chapter 5 and the data acquired in Chapter 7.

In an ideal transformer, the coupling coefficient k = 1 and the self-inductance is equal to the mutual inductance. However, in an inductive power transfer system this coupling factor is much lower, between k=0,2 and k= 0,06 and the mutual inductance's value is several times bigger than the self-inductance.

Once the mathematic expressions and principles of inductive coupling are known, it´s straight-forward to understand why does this kind of technology precise of high frequency signals.

As mentioned before, the inducted voltage is equal to the variation of the magnetic flux in a certain period of time, see equation (2.1).

This magnetic flux is the result of multiply the magnetic flux density by the area, equation (2.8)

$$\phi = B \cdot A \tag{2.8}$$

Since the current flowing through the windings is a sinusoidal wave, the generated magnetic flux density will also behave as a sinus, equation (2.8). Then, if the sinusoidal expression of the magnetic flux is replaced in equation (2.1) the result is that the induced voltage depends on the variation of the magnetic flux density (2.9).

$$B = \hat{B} \cdot \sin(wt) \tag{2.9}$$

$$emf = -\frac{d(\hat{B} \cdot \sin(wt))}{dt} \cdot A \tag{2.10}$$

The time derivative form of (2.10) gives an expression for the induced voltage that depends directly on the frequency of the magnetic field. That means that the higher the frequency, the higher the induced voltage, and consequently the amount of power transferred will be also larger.

$$emf = -\hat{B} \cdot A \cdot w \cdot \cos(wt) \tag{2.11}$$

2.3. Transformer's model and equivalent circuit

The physical phenomenon and its expressions explained on the former section let describe the air core transformer as a two inductors with its own self-inductivity L_1 and L_2, magnetically coupled with M as mutual inductance.

The equations (2.12) and (2.13) describe the resulting equivalent circuit.

$$U_1 = R_1 \cdot I_1 + L_1 \cdot \frac{dI_1}{dt} - M \cdot \frac{dI_2}{dt} \tag{2.12}$$

$$U_2 = R_2 \cdot I_2 + L_2 \cdot \frac{dI_2}{dt} - M \cdot \frac{dI_1}{dt} \tag{2.13}$$

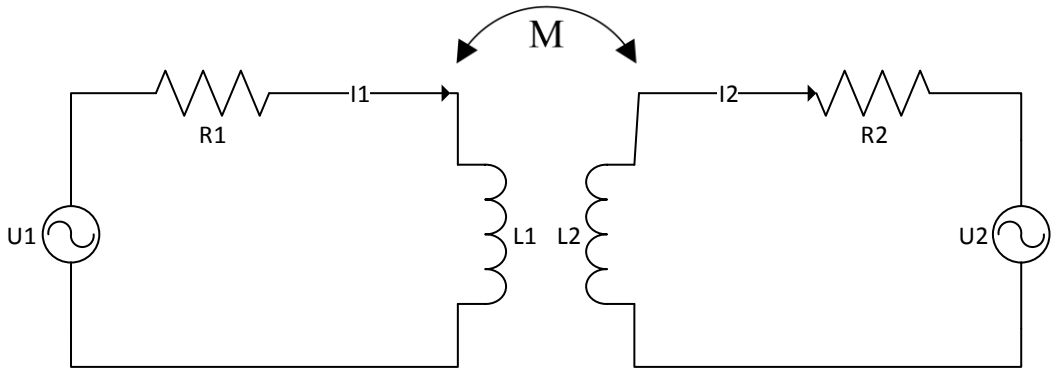

Figure 2.3 Equivalent circuit with magnetic coupling

2.4. Resonant circuit and compensation

2.4.1. Concept of resonance

In alternating current circuits where different passive elements coexist, like in the figure 2.4, the equivalent impedance can be calculated. This impedance is dependent on the values of each resistance, inductance and capacitance, but also on the frequency of the system.

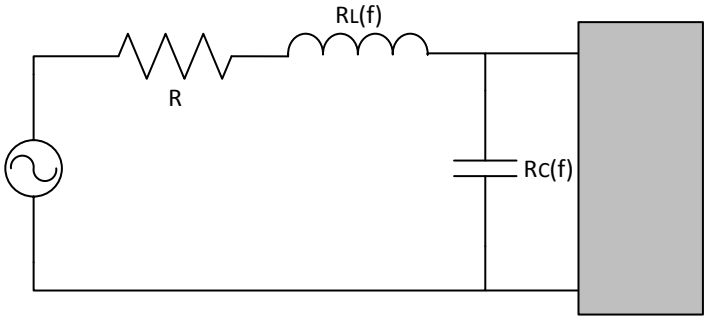

Figure 2.4 Example of a resonant circuit

The resultant impedance will consist of a real and an imaginary component, depending on the values of the inductances and capacitances of the circuit.

For a specific frequency, the impedance or the admittance will become null, when this happens, is said that the circuit is into electrical resonance (series resonance in the first case, parallel in the second) and this particular frequency it's called the resonance frequency.

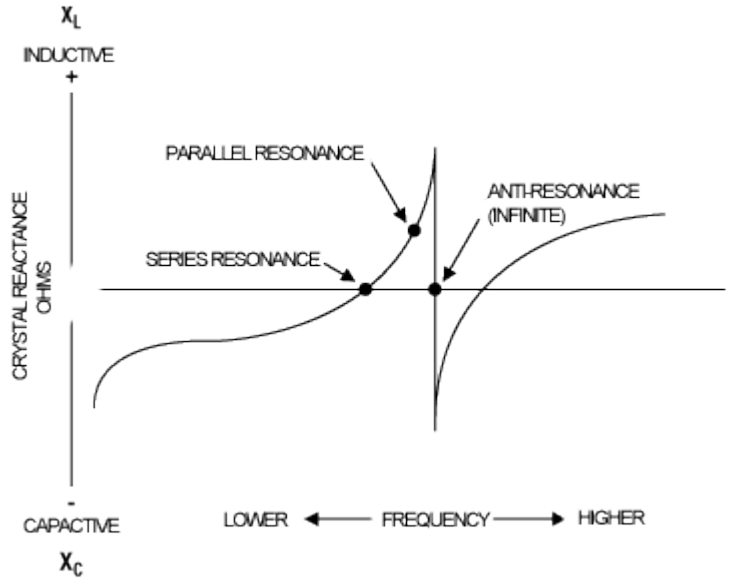

Figure 2.5 Example of series and parallel resonance [7]

In the case of study, the resonance that interest to archive is the first one, because annulling the imaginary component of the impedance will also imply that the power factor, $\cos(\varphi)$, will be next to 1 or 1 ideally. That means that the reactive power consumption will be zero, and all power consumed will be transformed to active power. That is the importance and the reason to look always for the resonant frequency of the system and work as close as possible to this frequency.

2.4.2. Capacitive compensation

Previous studies and description of compensation and circuit tuning methodologies can be found in [5] and [8]. This thesis focuses only in the chosen compensation method and its features.

As formerly mentioned, inductive coupling systems precise of reactive compensation in order to increase power factor and efficiency, to do it exist basically four types of compensation, Series-Series (S-S), Series-Parallel (S-P), Parallel-Series (P-S) and Parallel-Parallel (PP).

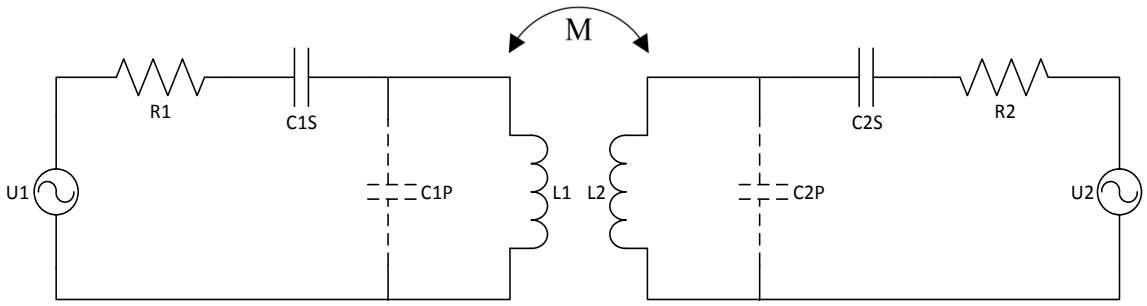

Figure 2.6 Different compensation topologies

Each compensation topology has its advantages and disadvantages, the selection of the most appropriate method will depend on the type of application and the features required. In the case of study, where the purpose of the wireless power transfer is to charge a battery or to feed a load, the most convenient will be the Series-Series compensation.

Drawn from [5] and [8], a primary parallel compensation imply current instability and precise higher control of electrical parameters. Besides, the parallel capacitor will need to stand the voltage drop of the primary side and also, variations in this voltage at high frequencies will generate high dangerous currents.

In contrast to the parallel, the series primary compensation is more stable against frequency variations and capacitors don't have to stand greater voltages or currents than the nominal ones. Furthermore, series compensation in primary winding is chosen so that the impedance as seen from the source side is purely resistive in nature. That means that the

load will reflect only its real component and the reactive power consumption will be minimized.

Regarding the secondary winding's compensation, the series topology reflects no reactance at the nominal resonance frequency, which means that the first inductor can be tuned out independent of either the magnetic coupling or the load.

As a brief summary, the main reasons to select the Series-Series compensation are:

- Load-independent phase gap between voltage and current inputs
- Load-independent current source
- Primary and secondary compensation capacitors independent of either M or load
- Secondary winding reflects only real component as impedance
- S-S compensation is appropriate for battery charging since it behaves as a current source and can be easily adapted to do it as a voltage source.

2.5. Power electronics

The main purpose of the power electrics is to transform the input electrical signal, voltage and current, to a different output, whether in terms of amplitude, frequency or type (AC or DC). This is possible due the static commutation of the semiconductors that adapts the input signal to the desired output.

2.5.1. The inverter

Detailed information about the inverter and its design and construction can be found in [4].

The inverter is the responsible to modulate the wave from the grid to a desired output, as already mentioned can generate AC waves with frequencies from 50 to 500 kHz, adapting the switching frequency to the resonance frequency of the system.

The converter's structure is modular, which means that the inverter can work either in half-bridge structure or full-bridge. Besides, this modularity reflects advantages in terms of heat dissipation and repairing tasks.

One important feature is the capability of performing Zero Voltage Switching (ZVS) and Zero Current Switching (ZCS) when working at resonance frequency, which reduces remarkably the power losses but introduces two possible working cases to take into account. The inductive load case and the capacitive load case.[4]. Besides, another important advantage for ZVS as well as ZCS is that reduces remarkably the electromagnetic interferences produced by the commutation of the inverter.

If the inverter is commutating at frequencies lower that the resonance frequency of the system, the load seen by the source it's capacitive in nature and that implies that the current wave has a negative phase gap in reference to the voltage wave. In this case, every time that the converter commutates, a high du/dt and consequently an also high di/dt will be generated in the transistors. When this happens, greater power losses are generated and ultimately, that affects to the efficiency and the proper functioning of the converter. Contrary to the capacitive, in the inductive load case this behaviour doesn't take place.

Therefore, always will be preferable to work in inductive load case, as close as possible to the system's resonance frequency.

The elements that make up the inverter itself can be seen in the figure 2.7. Attached to each heat-sink lay the HB Platine (Half-bridge PCB) with the semiconductor's connexions. Over it the Treiberplatine (Drivers PCB) can be seen, contains all the drivers IC needed to generate the proper pulses to the MOSFETS gates. The whole system is controlled by the Steurerungsplatine (Control PCB) and the information between the power and the control parts is send and received using optic fibre connections.

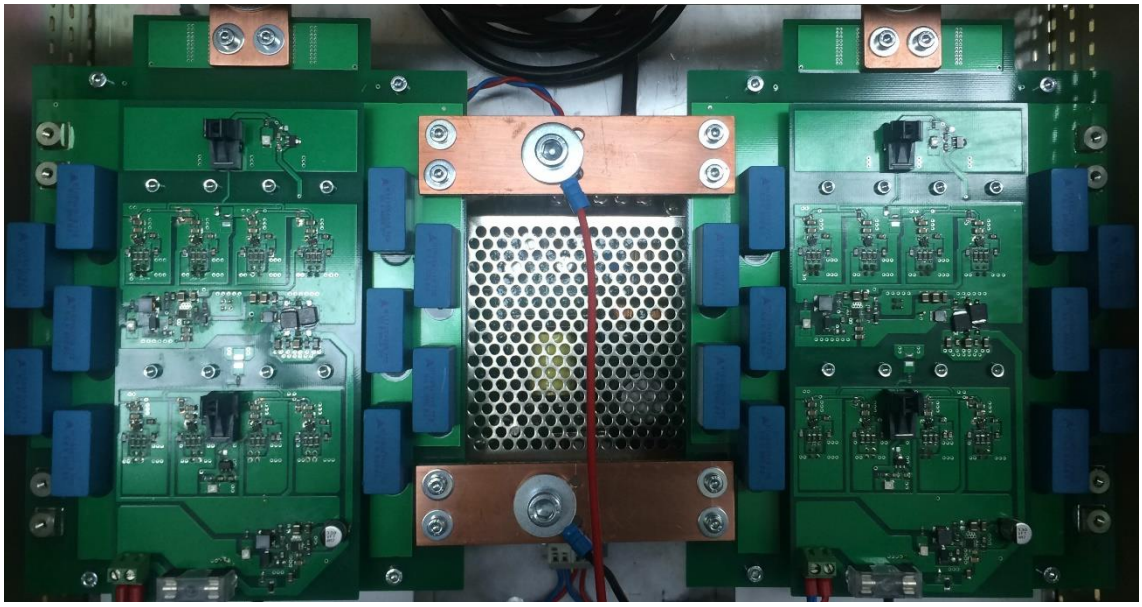

Figure 2.7 Arrangement of the two half-bridge inverter PCB

The final construction can be seen in figure 2.8

Figure 2.8 Final construction in closet

2.5.2. The secondary rectifier

Once the electrical signal has been transferred from the primary winding to the secondary, the result is an alternating current wave which is not suitable to use it to charge a battery pack. The reason is because a battery is a unipolar voltage source and connecting it to an alternating source will generate a short circuit that could damage or even destroy the system.

The solution is then to transform this wave to a direct current wave by means of a rectifier.

2.5.3. Rectifier's power losses calculation

Two types of power losses can be distinguished regarding the operation of a diode. The conduction and the switching losses. [10]

Conduction losses

The conduction losses in a diode appear when the diode is in forward conduction mode due to the on-state voltage drop (U_F). Most of the time the conduction losses are the main contributor to the total diode power losses and the junction temperature rising.

The conduction loses are described by the equation (2.14).

$$P_{Fc} = \frac{1}{T} \cdot \int_0^T U_F I_F \, dt = \frac{1}{T} \cdot \int_0^T (V_{TO} + rtI_F) I_F \, dt = V_{TO} \cdot I_{Favg} + rt \cdot {I_{Frms}}^2 \quad (2.14)$$

Where I_{Favg} and I_{Frms} are for a single phase rectifier:

$$I_{Favg} = \frac{I_{Fmax}}{2} \quad (2.15)$$

$$I_{Frms} = \frac{I_{Fmax}}{\sqrt{2}} \quad (2.16)$$

Where I_{Fmax} is the highest current through the load.

Switching losses

If a reverse voltage across the diode is applied, current through the diode comes to zero value, and the diode continues to conduct in the opposite direction because of the presence of stored charges in the depletion layer and the p or n layer. The diode current flows for a reverse recovery time t_{rr}. This is the time between when the instant forward diode current becomes zero and the instant reverse recovery current decays to 25 % of its reverse maximum value.

They can be calculated using the equation (2.17).

$$P_{Fs} = Q_{rr} \cdot Ur \cdot f \tag{2.17}$$

2.5.4. Three-phase rectifier, DC-Link and Safety hardware

The remaining hardware of the system are the Three-phase rectifier of the primary winding, which rectifies the grid signal and feeds the DC-Link.

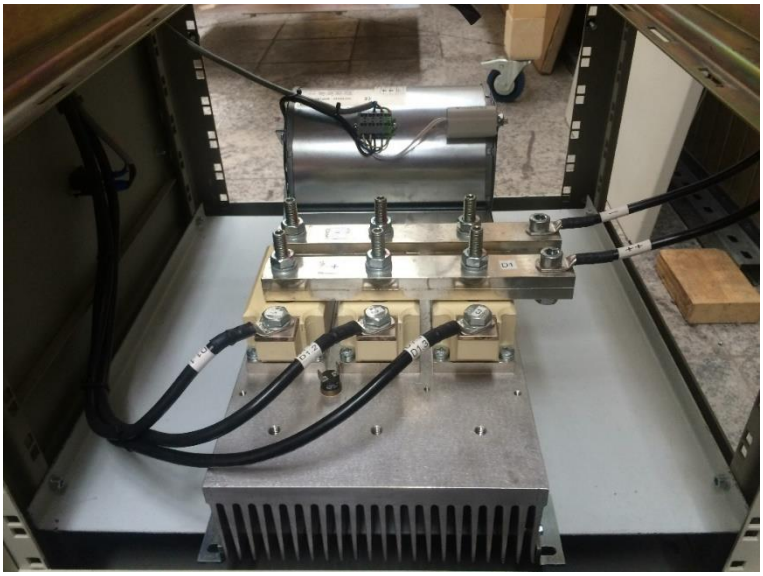

Figure 2.9 Three-phase rectifier

The DC-Link if configured by means of 9 capacitors resulting a total of 4 mF.

Figure 2.10 DC-Link

The figure 2.11 shows the remaining components of the enclosure, including the safety relays and contactors.

Figure 2.11 Relays and contactors of the enclosure

3. Software

In this chapter the software of the power inverter designed in [4] will be described, starting with the explanation of the software structure, the state machine and the PWM generation. Subsequently the design and implementation of the Pulse-test and the monitoring technology will be described. More information about the software can be found in [4] and [14].

3.1. Software's structure

As can be read in [4] the system is driven by a main Electronic Control Unit (ECU) that controls the system's state machine, the PWM generation and performs the surveillance of the critical variables measurements.

This ECU uses the ATMega 324-P microcontroller and for the PWM generation the Altera MAX3064A for both ICs a clock frequency of 20 MHz is set.

The PWM signal frequency can be set between 37 and 487,8 kHz using the potentiometer installed in the user interface. The duty cycle can be also set from 0 to 100 % by means of a second potentiometer.

The most important variables as well as the current status of the state machine can be controlled and seen in the LCD display of the users interface. To move forward through the different status the user can press the confirm button and can select the mode of operation using a mode selector. Details of the user's interface can be seen in the Figure 3.1.

Figure 3.1 User's interface

In order to perform a safe and correct start-up of the system, the software follows a structure based in status, when the change conditions are fulfilled, the system moves forward to the next status. If any error occurs the system moves to an error status, when the system's conditions are safe again the program will be restarted. More information about the state machine can be found in [4].

The mentioned status are:

- Status 0 or Boot:
  Control and Power parts of the system must be powered, to move to the next status the modes selector must be set to position 1 or 2 and the potentiometer values for frequency and duty cycle must be set to maximum and minimum respectively.

- Status 1 or Confirm:
  Confirmation by means of the press button during one second.

- Status 2 or Choose mode:
  There are two modes of operation, Half-bridge and Full-bridge. This modes are related to the inverter's structure, the selection of the modes is done using the modes selector in position 1 for Half-bridge or 2 for Full-bridge.

- Status 3 or Pulse-test:
  In this status, the calculation of the system's resonant frequency is performed. Once the calculation is done, the user must set this frequency using the potentiometer and confirm in order to move to the next status. More information about the Pulse-test can be found in section 3.2.

- Status 4 or Active:
  The system is ready to charge. The PWM generation is activated and the system supplies power accordingly to the duty cycle selected.

- Status 100 or Error:
  If any error occurs at any time or a malfunction is detected, the system goes to this status where the PWM is disconnected. If the failure is solved, the system moves to status 0. The system's shut down is performed under soft switching conditions, using the current's zero crossing signal, that avoids possible damaging of the components and other related issues due high voltage and current variation.

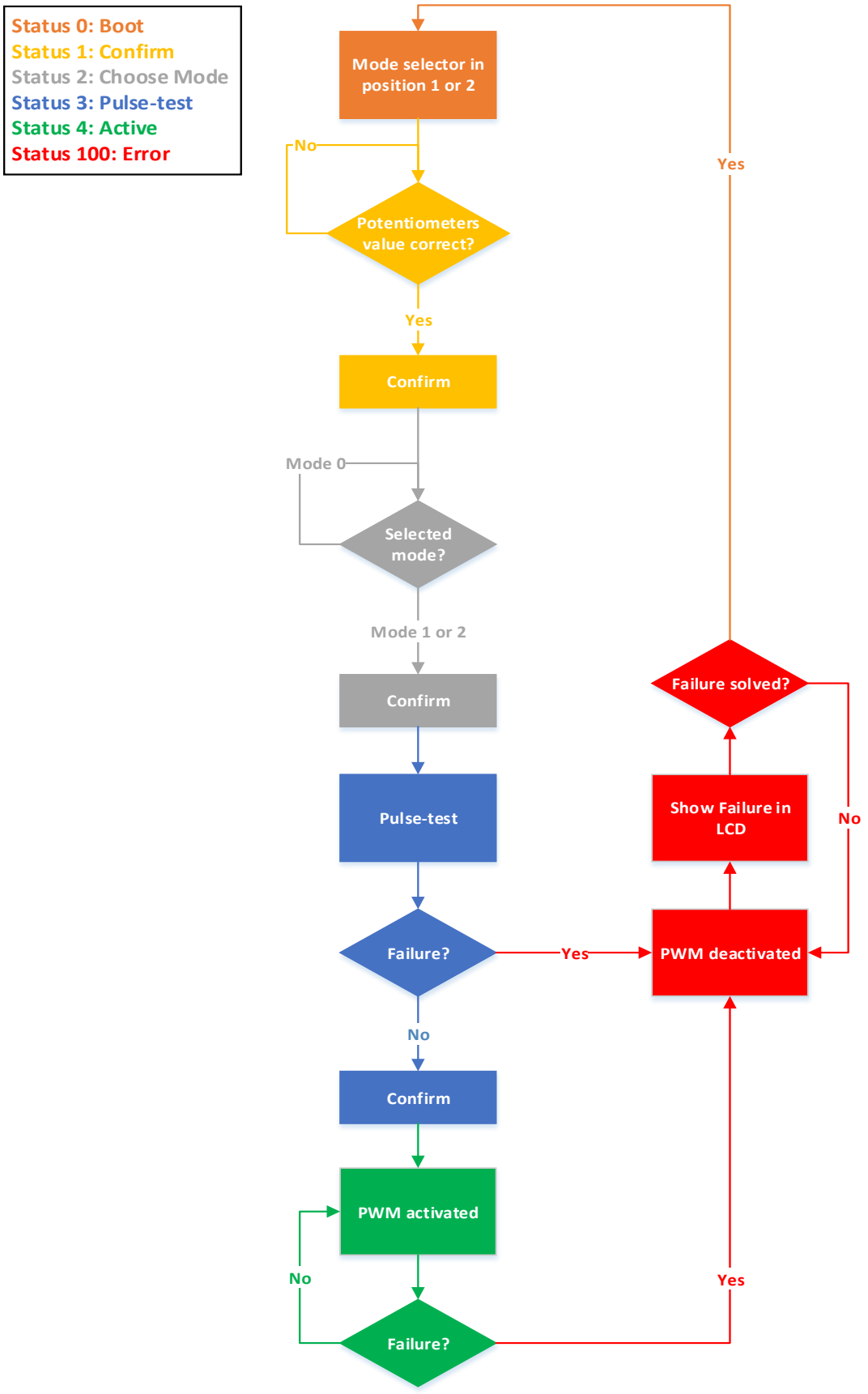

Figure 3.2 State's machine flow chart

3.2. PWM generation

As previously mentioned, one of the features of the power inverter is the capability of generating an AC signal with frequencies from 50 to 500 kHz.

This PWM signal that controls the MOSFETS commutation is generated by the microcontroller by means of the Timer 1, this timer is set in CTC Mode (Clear Timer on Compare Match) and the frequency is selected using the ICR1 register which imposes the maximal value (TOP) for the Timer 1 register, TCNT1. Since the timer will be counting without prescaler, every cycle will run at 20 MHz and the minimal value for the ICR1 register will be 40 (for 500 kHz PWM).

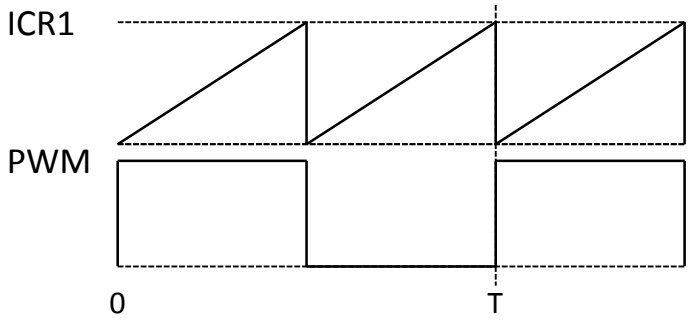

Figure 3.3 PWM generation

According to the microcontroller's datasheet [14], when changing the TOP value the program must ensure that the new TOP value is higher or equal to the value of all the Compare registers. Otherwise, the Compare Match will be missed and the counter will count until MAX (0xFFFF). If ICR1 is used, must be for a constant frequency operation when the value of this register will never be changed. For this and other reasons it is important to calculate the resonant frequency of the system before starting its operation.

Two output signals, related to pins OC1A and OC1B, are used in the PWM generation. To set the desired duty cycle, a phase gap between both signals is used. The first one will always have a constant phase while the second one will change it.

The relation between the frequency and duty cycle registers can be seen in equation (3.1)

$$OCR1B = \frac{ADCduty\ cycle\ value \cdot ICR1}{1000} \tag{3.1}$$

For instance, for a 500 kHz, 50% duty cycle output, the value of ICR1 will be ICR1 = 20 and OCR1B = 10.

Each PWM signal generated by the microcontroller belong to the high side of each inverter's half bridge. The corresponding signals for the low side are generated by means of a CPLD,

which also applies the dead time those signals. As already said, the duty cycle can be controlled through the variation of the signal's phase gap between both high sides, where 0º is equal to duty cycle null, and 180º the maximal duty cycle, 100%.

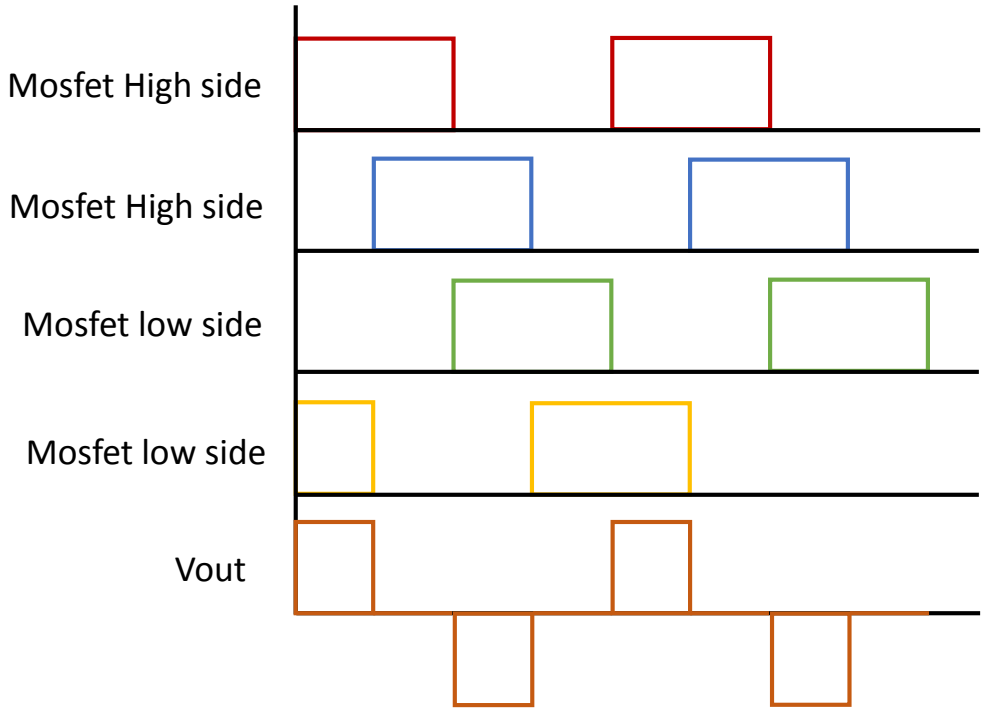

Figure 3.4 Example of PWM with 50% duty cycle

During the development stage of the PWM's software, some issues regarding the correct functioning of the routine had to be solved. Due the timer's configuration, the registers ICR1, OCR1A and OCR1B were no double buffered. As consequence, when the values of these registers were changed while the timer was running, it could happen that the register's update was delayed or anticipated one clock. Therefore, the PWM signal was inverted, the phase increased 180º and the duty cycle was absolutely different. For instance, for a duty cycle of 5, the system would suddenly work at 95 % of its capacity. This situation presented a high risk for the system as well as for the load, and had to be solved.

In order to do it, a routine regarding the PWM register's update was implemented, ensuring that the register's update was performed within a "secure range", this range of values that ensured that the timer won't miss the update, and all this process done as an atomic operation to ensure that no other commands will be performed during this process.

The result was an operable and safety software that performed the register's update efficiently and failure free. Nevertheless, to ensure the best system's functioning it's strongly recommended to perform little steps when changing the duty cycle as well as the frequency. The lower the step, the higher the secure range to perform the register's update.

3.3. Monitoring and surveillance technology

In electrical and electronical systems there are some critical variables that have to be controlled and supervised periodically, to ensure the proper functioning of the system, the following factors are controlled. More information can be found in [4].

3.3.1. Temperature

One of the major problems when talking about power electronics is temperature and power dissipation. To have it under control, three NTC temperature sensors are used, one for each inverter's heat-sink and the third for ambient temperature control.

When an over temperature is detected reading the signal received in the ADC, the system moves to the Error status, protecting itself and stopping the operation.

The main change in the program was to implement the NTC equation and implementing the routine that constantly compares this value with the maximal temperature allowed. Once the temperature gets too high, the system will recognise this failure, will show it in the display and will switch off the power.

3.3.2. Voltage

The main problem related with voltage is a possible over voltage that could damage, and even destroy, the system. Voltage is also controlled by means of a voltage sensor and it value is read in the ADC and processed by the microcontroller.

3.3.3. Current

Current is also one of the main important factors to control since is responsible of power dissipation and related temperature problems.

The system receives several current measurements that lets avoid damages or even elements destruction. This signals are the RMS current value and two amplitude error signals, one for the positive semi period and another for the negative.

Using this signals it's possible to establish a current control to choose the charging current of the system and also a maximal value current error. This error will turn off the system moving the software to the Error status.

Another important aspect that it's also monitored using the current sensor is its zero crossing signal. A pulse signal will indicate when the current wave crosses the zero. This function will enable to perform the calculation of the resonant frequency of the system and also will allow to turn off the system using a zero current switching technique. This technique

reduces the power dissipation of the power electronics, ensures a proper switch-off of the system and increases the element's life.

Besides, the zero crossing signal is used to perform a secure switch off of the system in case of failure. Once a failure is recognise, the system will wait for a zero crossing signal and then will switch off the power. That way possible voltage and current peaks and its consequences can be avoided.

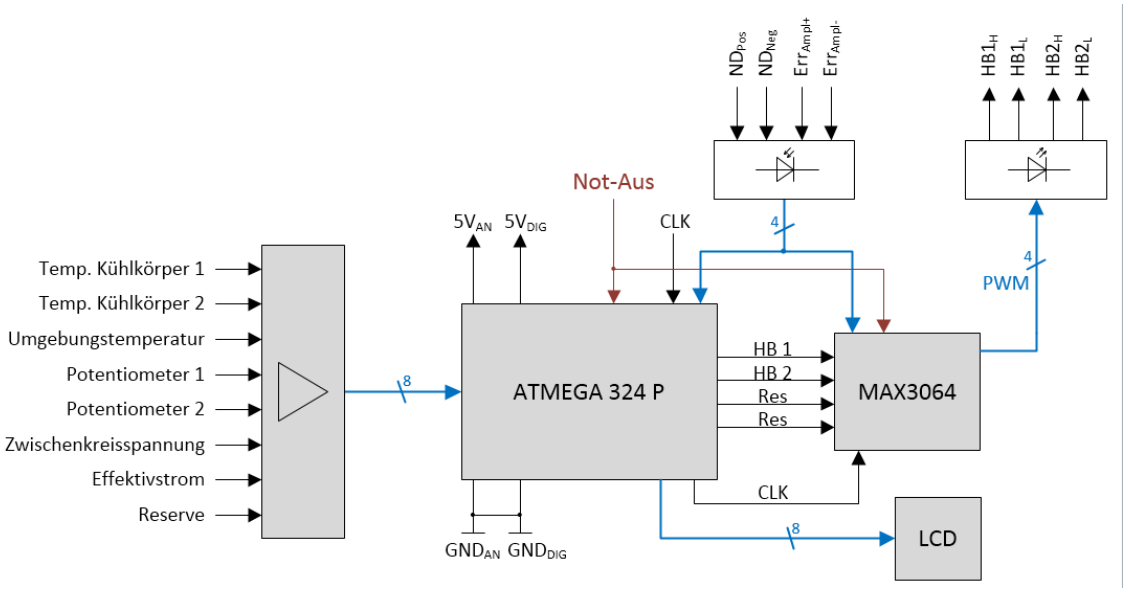

Figure 3.5 Measurement and surveillance technology

3.4. Pulse-test

In the section 2.4 the importance of working at the resonant frequency of the system has been already explained. For these reasons a methodology to perform the system's resonance frequency calculation has been implemented, this is the main purpose of the Pulse-test status.

3.4.1. Methodology

The methodology chosen to do it, is to "hit" the system generating a voltage pulse, and afterwards by means of a current sensor to identify the frequency with which the system is vibrating, the resonant frequency. In order to be able to track the current signal, the zero crossing signal described in 3.2 will be used.

3.4.2. Pulse-test's software

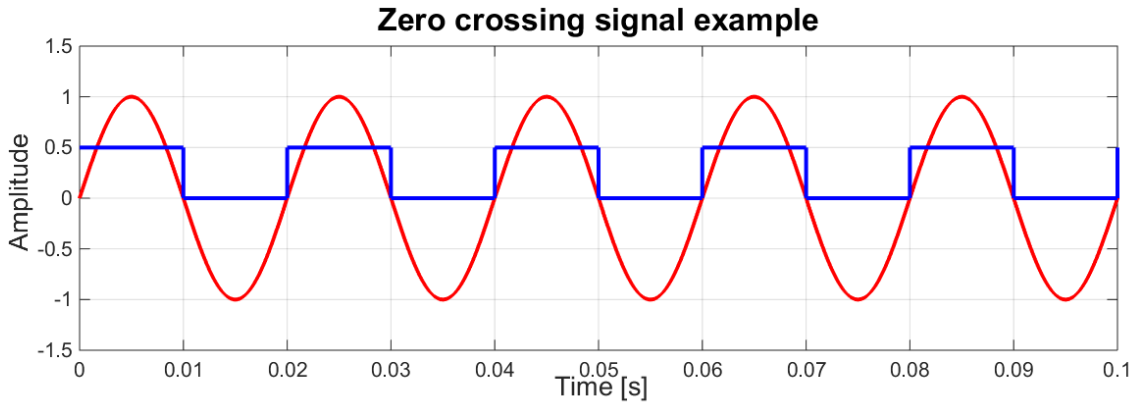

Figure 3.6 Theoretical example of the Pulse-test

The software's main objective in this status is to recognize the signal's frequency received from the optical link device.

To do it, in first place the PWM will be activated in order to generate the voltage pulse needed. Once the pulse has been produced, by means of pin polling technique the rising edges of the received zero crossing detection signal will be recognized and counted during a certain period of time.

Then, the frequency is calculated by dividing the number of rising edges by the calculation time. This result will be displayed afterwards on the LCD.

One of the biggest problems detected when implementing the routine, was the impossibility of recognising signals with higher frequencies that 400 kHz. Due the Nyquist theorem, the sampling frequency needed to be at least 2 times bigger than the signal, for this reason,

due the time needed for the system to perform the pin polling and comparing operation, the maximal frequencies available to be recognised are up to 400 kHz.

There are some solutions for this issue. If it's desired to work with the same microcontroller, the Timer 1 can be set in Capture mode [14]. This way the microcontroller operates the frequency recognition completely with hardware, and the process will be much faster.

Another solution could be to use another microcontroller capable of working at higher frequencies, that way the clock operations will be performed faster and so will be the pin polling operation.

The figure 3.7 shows the software's flow chart implemented in the Pulse-test routine.

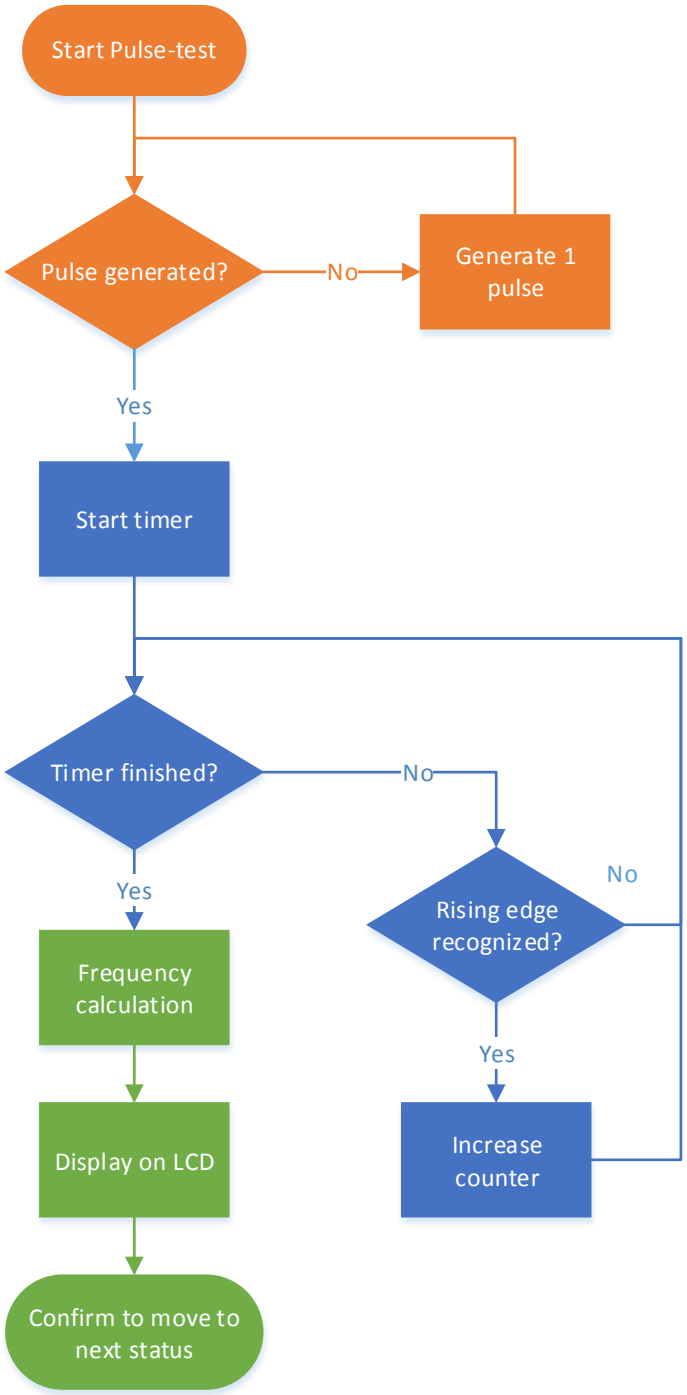

Figure 3.7 Pulse-test's flow chart

4. Hardware

In this chapter, the system's remaining hardware left to implement is explained. More precisely, it describes the design and construction of the secondary winding's passive rectifier and its filter and the construction of the capacitors compensation module. Together with the information that can be found in [4] and [5], all information regarding the system's hardware is completed.

4.1. Passive rectifier

There are many different kinds of AC/DC converters, in the case of study the single phase full bridge passive rectifier structure has been selected.

The four rectification units are composed by 32 diodes, 16 semiconductor modules arranged by 4 modules per unit. The diodes are based in the SiC technology which application is very appropriate in high frequency systems since their recovery charge is almost negligible, which means that the switching losses can be neglected. The maximal junction temperature is also high, the semiconductor can stand temperatures up to 175ºC and thus a working condition of 140ºC can be set without component deterioration.[14]

A schematic of the connections and the modules arrangement as well as the filter can be seen in figure 4.1.

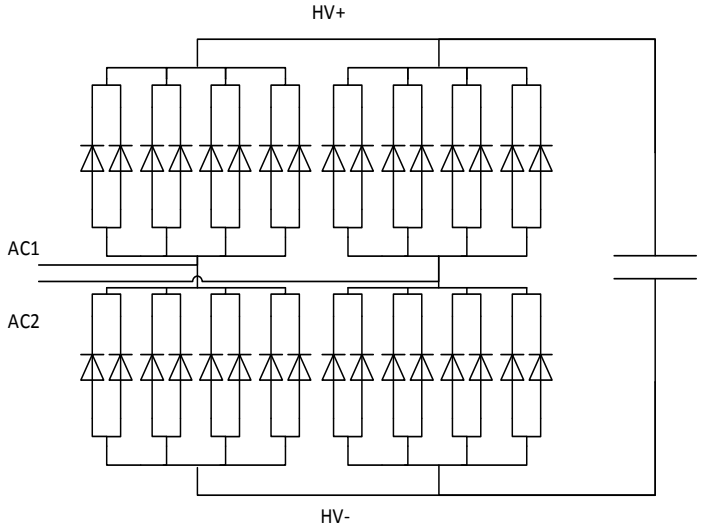

Figure 4.1 Secondary rectifier schematic

4.1.1. Power losses calculation and heat sink size

To calculate the power losses in the converter the expressions discussed in the section 2.5.3 have been used.

The values of V_{T0} and r_t have been calculated from the diode model given by the manufacturer in the datasheet. For a T= 100ºC, V_{To} = 0,837 V and r_t= 0,115 Ohm.

Then, for an I_{Fmax} of 10,25 A for each diode (there are 8 diodes in parallel in every unit of the rectifier) the I_{Favg} = 5,125 A and I_{Frms} = 7,24 A.

With all the values the power losses can be now calculated, equation (4.1).

$$Plosses/diode = V_{To} \cdot I_{Favg} + rt \cdot I_{Frms}^2 = 0{,}837 \cdot 5{,}125 + 0{,}115 \cdot 7{,}24^2 = 10{,}5\ W \quad (4.1)$$

$$Plosses\ total = Plosses/diode \cdot 32 = 340W \quad (4.2)$$

Once the power losses have been calculated, it is turn to size the heat sink that will dissipate the generated heat letting work the converter in a safety range of temperatures and conditions. To do it, the thermal resistance of the circuit must be calculated and this implies to know the thermal resistance of the semiconductors as well as the thermal resistance of the heat sink.

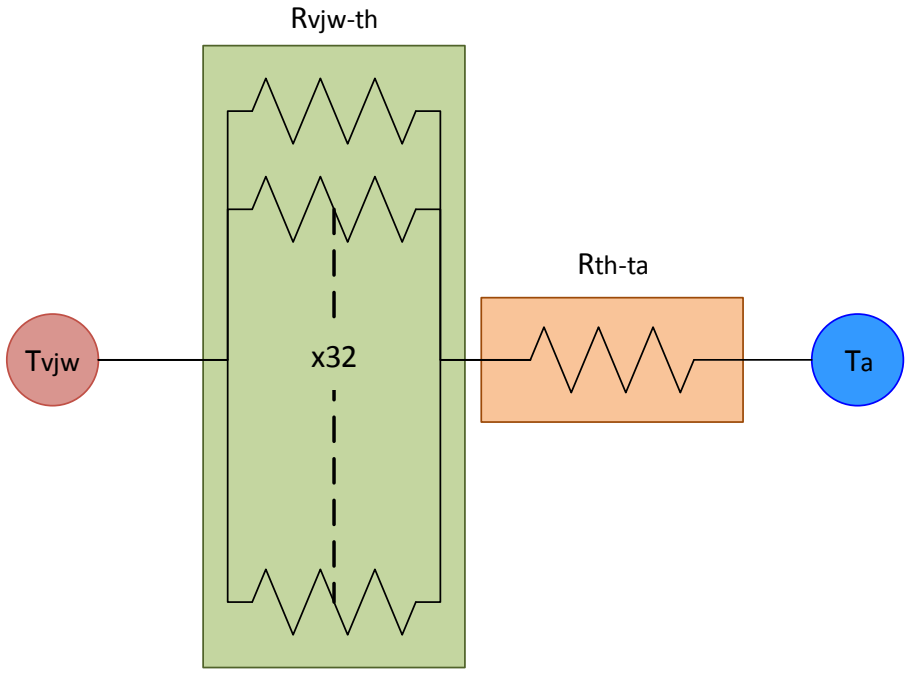

Figure 4.2 Thermal circuit of the rectifier

Drawn from the thermal circuit, the heat sink's thermal resistance (Rth-ha) can be calculated using equation (4.3).

$$Rth - ha\ max. = \frac{(Tvjw\ max.\ \cdot 0{,}8) - Ta}{Plosses\ total} - \frac{Rvjw - th}{\#diode} = \frac{(175\ \cdot 0{,}8) - 50}{340} - \frac{1{,}5}{32} = 0{,}22\ ºC/W \quad (4.3)$$

Due sizing issues the final heat sink used is the LAV 7 200 from Fischer Elektronik which is bigger and has a lower thermal resistance (0,08 ºC/W). Thus, the safety coefficient for the rectifier's warming has been increased. Ensuring the proper functioning of the converter.

4.1.2. Simulations

The simulations performed let to have an idea of the rectifier's behaviour in the system's global environment.

In order to reduce current and voltage ripples a C filer has been implemented. As can be seen in figure 4.3, the ripple after the filter at 85 kHz it's almost negligible.

Another important parameter to take into account when sizing the filter is the current through the C filter, which indicates the RMS current that the capacitors must be able to withstand.

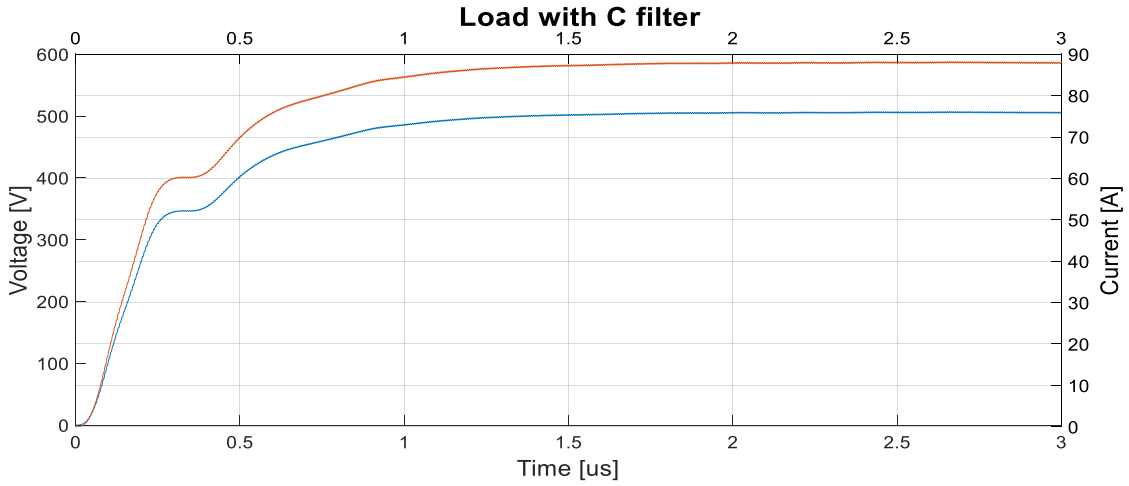

Figure 4.3 Current and voltage through load with C filter

Drawn from the simulations, the capacitor chosen it's the MKP1848, from Vishay recommended for DC-Link applications. With a capacitance of 8 µF, the filter will be composed by an array of 7 capacitors in parallel. [15].

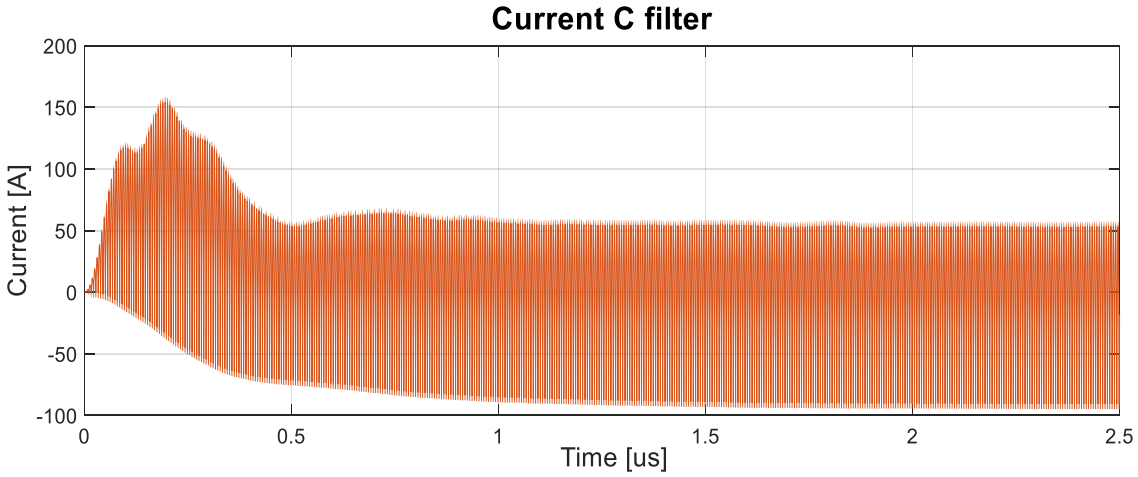

Figure 4.4 Current through C filter

4.1.3. Design and Construction

The strategy chosen in rectifier's design is a modular structure, suitable to adapt and implement future changes if needed. The concept is simple, the rectifier consists of two PCB, one with the diode arrays and the other with the filter. The width of every trace is sized to avoid high temperature rises. Furthermore, a copper depth of 70 µm has been selected for the diode PCB.

The resulting PCB for both can be seen in figures 4.5 and 4.6. In figure 4.7 the complete construction of the rectifier is shown.

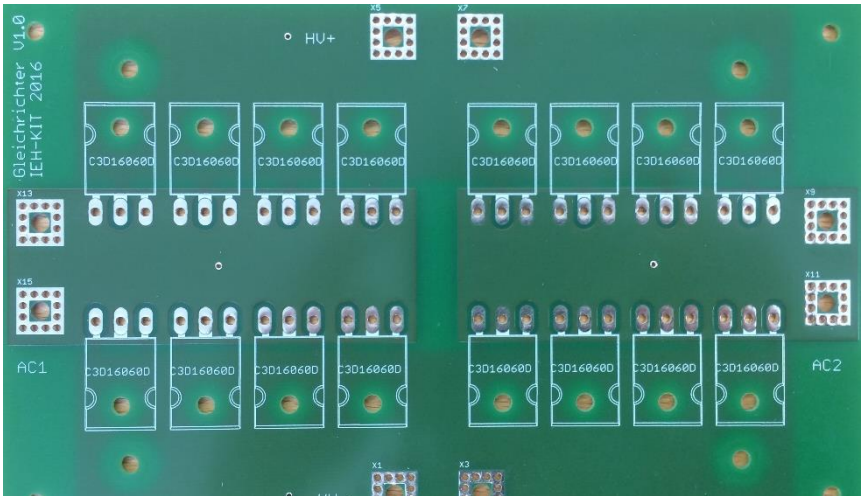

Figure 4.5 Diodes PCB

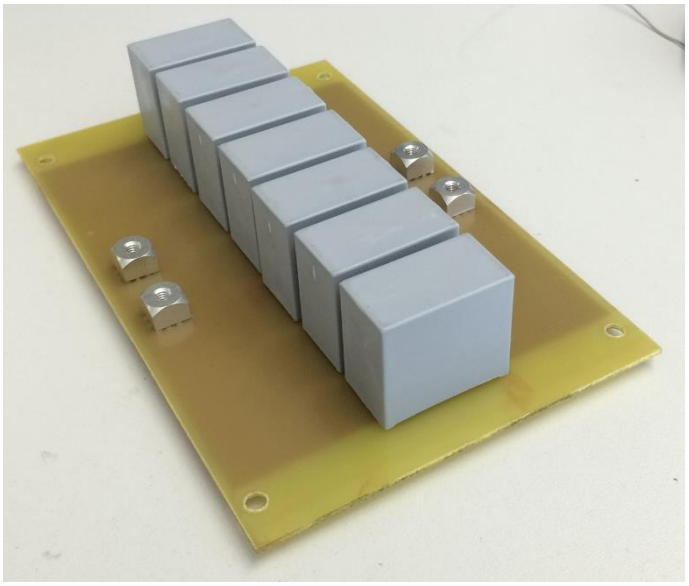

Figure 4.6 Filter PCB

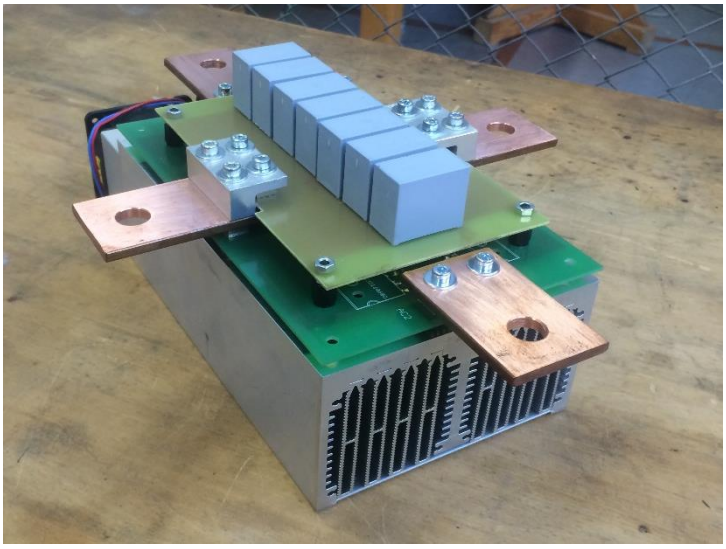

Figure 4.7 Complete secondary rectifier

4.2. Capacitive compensation

Drawn from previous studies and calculations performed in [5], the capacitance, the model as well as the number of required capacitors for every system under testing were known.

The selected component is the Celem CSM 150 [12] and the reasons for its selection is their flexibility in terms of frequency properties and that regarding calculations in [5] allows to maintain a low number of capacitors for almost every needed array and system under test.

The table 4.2 summarizes the information regarding the built compensation module and the differences between the theoretical values and its consequences for a theoretical resonance frequency of 85 kHz.

System	32.1	61
C1 theoretic capacitance [nF]	29,77	121,31
C1 real capacitance [nF]	30	133,33
C2 theoretic capacitance [nF]	82	75
Theoretical resonance frequency [kHz]	85,891	85,531
Real resonance frequency [kHz]	87,67	81,585
Difference [%]	2,1	4,61

Table 4.1 Theoretical and real capacitances and its effect in the resonance frequency

The construction of the modules has been done by means of square aluminium rods connecting several capacitors with each other. In figures 4.7 and 4.8 the arrays for the system 32.1 can be seen. Each compensation module is placed in a wood enclosure with the appropriate dimensions to be suitable for both systems and every resonance frequency.

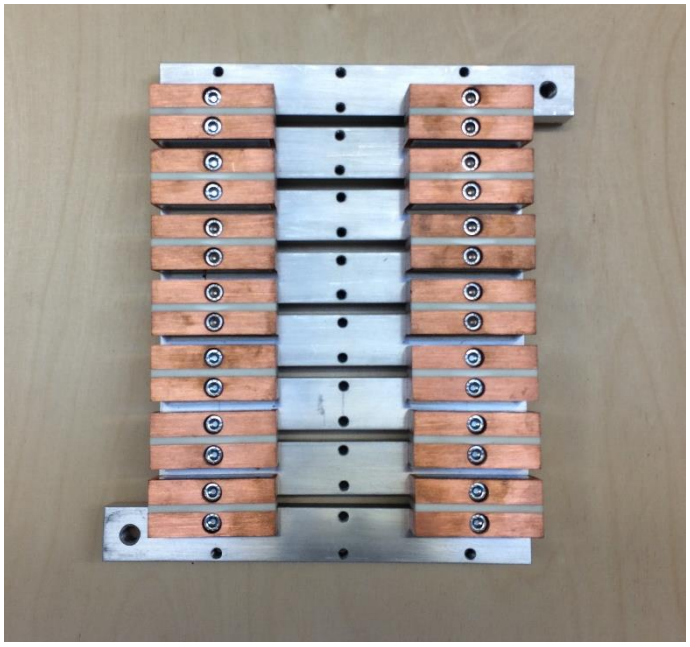

Figure 4.8 Primary winding compensation module

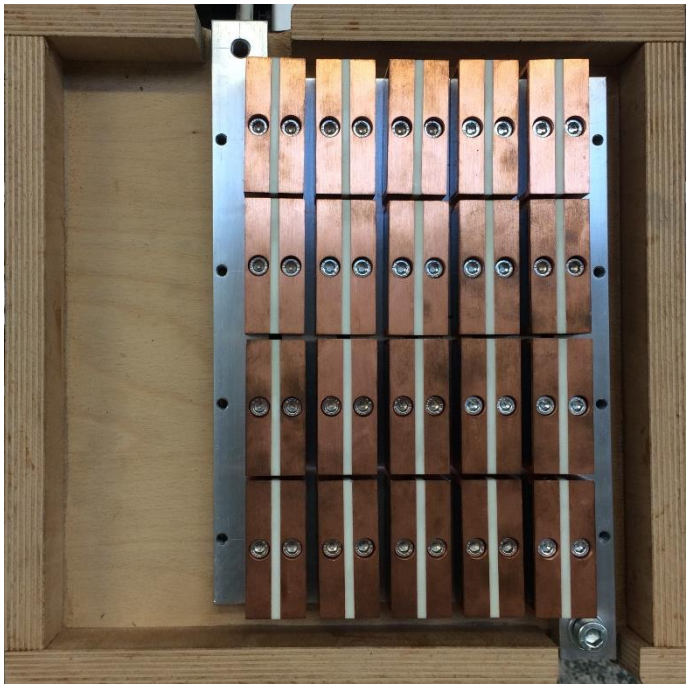

Figure 4.9 Secondary winding compensation module

5. Measurements and results

This chapter describes the obtained results from the tests performed to the different designed elements and the whole system altogether.

5.1. Test bench

In order to take all the measures and test the several systems the test bench developed by [9] has been used. The structure is a 3-axis-controlled system which lets set both windings at different distance and offsets.

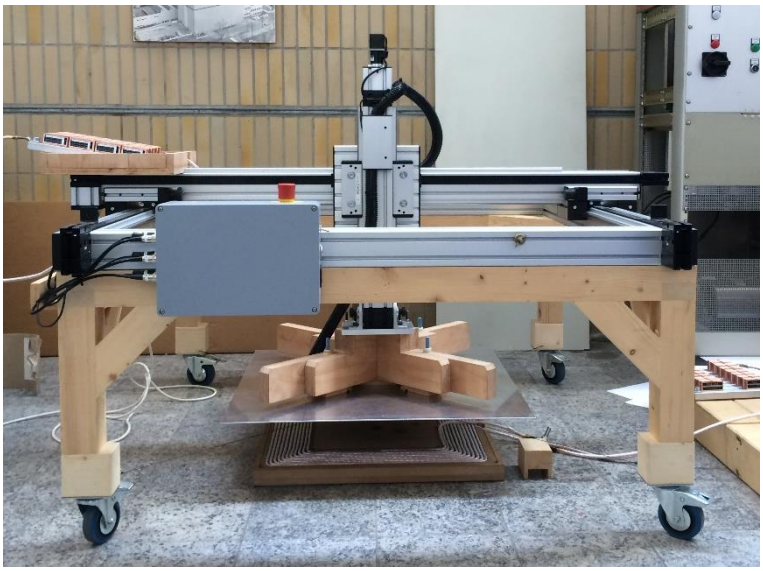

Figure 5.1 Complete test bench's structure

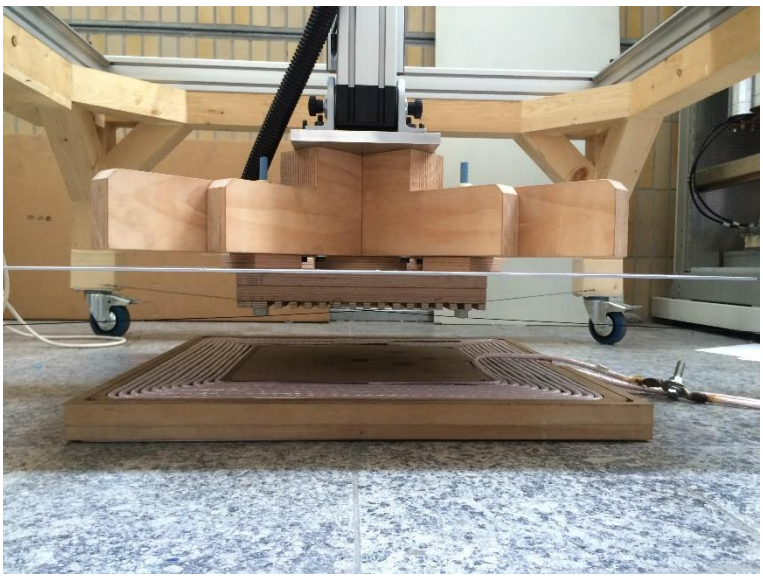

Figure 5.2 Positioning detail of both windings

5.1.1. Measuring devices and power sources

The measuring devices and power sources used in the stage of validations and start-up are:

- Fluke 177 True RMS Multimeter
- Oscilloscope Tektronix MDO3034
- Pearson Current Sensor M110
- Hameg differential probe HZ115
- ZES Zimmer LMG 500
- Heinzinger transistor-netzgerät TN 100-1000
- Hioki LCR meter 3522-50
- Omicron Bode Analyser 100

5.2. Pulse-test

5.2.1. System 69,4 kHz

The first tests have been performed using the system of the figure 5.3, the aim of this tests are to demonstrate the proper functioning of the system, the PWM software and the state machine as well as the pulse-test methodology. The Bode Analyser device has been used to know exactly its resonance frequency, 69,4kHz. The results of the frequency sweep analysis can be seen in figure 5.4.

Figure 5.3 System 69,4 kHz

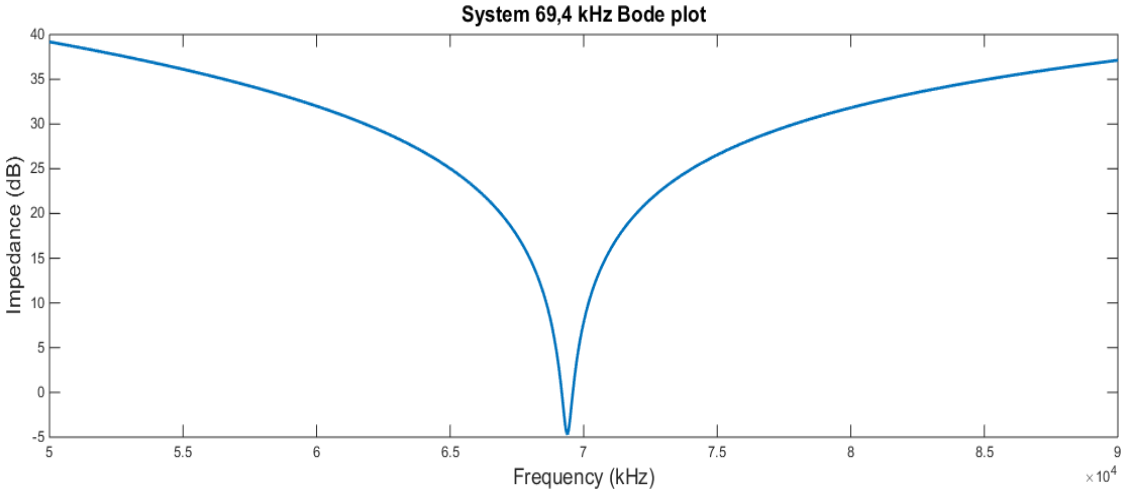

Figure 5.4 System 69,4 Bode plot

The first Pulse-tests were performed with an output signal of 200 kHz but due the high inductivity nature of the system in this conditions, the current generated was not high enough and the voltage showed high irregularities and peaks that could damage the power electronics. Drawn from this results, the following tests were performed using an output signal's frequency of 50 kHz.

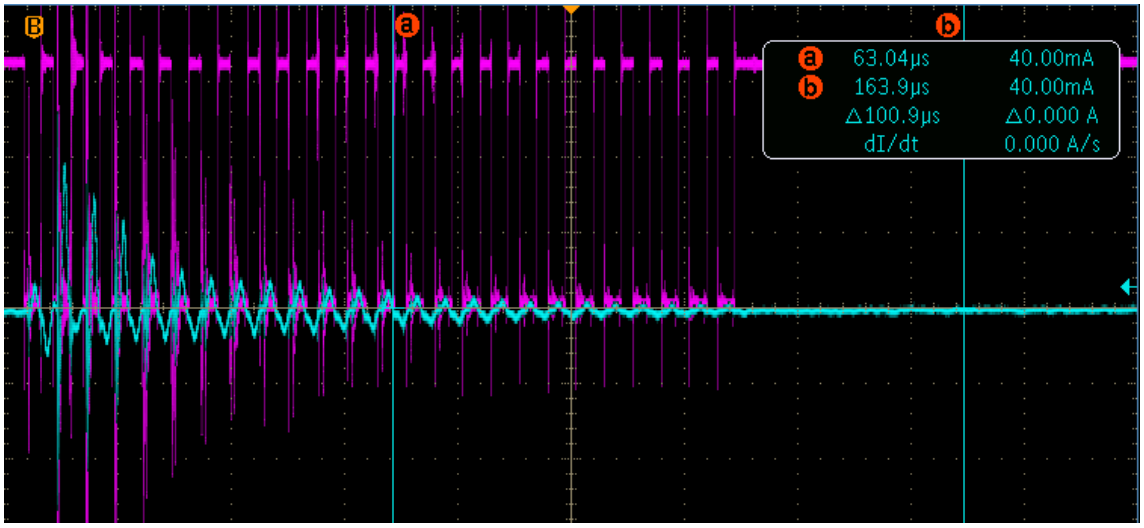

Figure 5.5 Pulse-test at 200 kHz

At 50 kHz, it can be seen how after the train of pulses generated by the inverter, the current frequency changes, and the system vibrates at the resonance frequency (Figure 5.6).

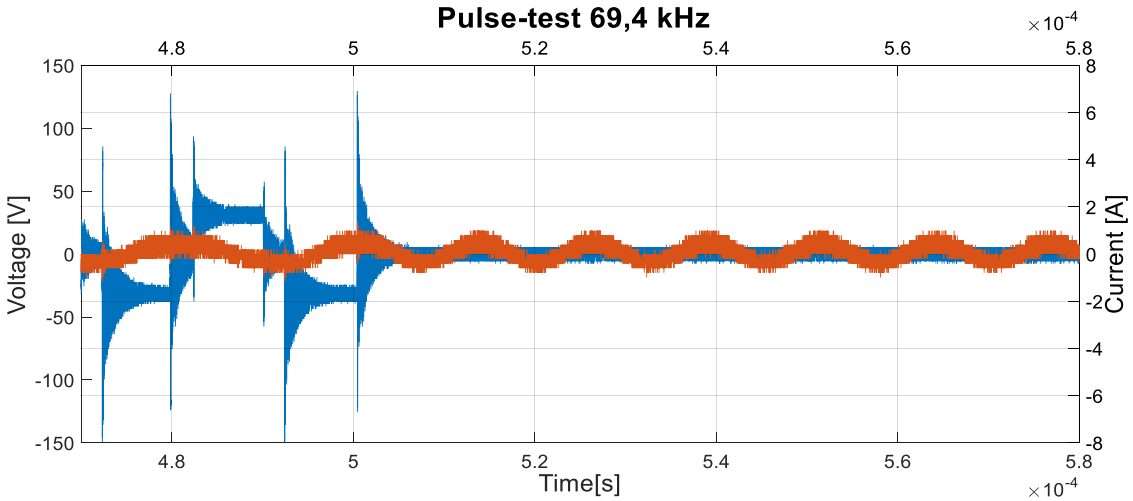

Figure 5.6 Pulse-test with 50kHz initial frequency for the system 69,4 kHz

As result of this firsts tests, the following conditions for the Pulse-test were established:

- Signal's frequency = 50 kHz
- Train of pulses length = 400 µs

5.2.2. Systems 81- 97-148 kHz

Once the proper functioning of the system was ensured, the following step was to prove the pulse-test methodology for different resonance frequencies and voltages with the objective of establishing the operative conditions of this pulse-test to be valid, no matter the system under testing.

To do it, the assembly of the figure 5.7 was built, and the various frequencies were set changing the total capacitance of the capacitor bank.

Figure 5.7 System 148 kHz

The following figures show some of the most representative results obtained during the several tests performed.

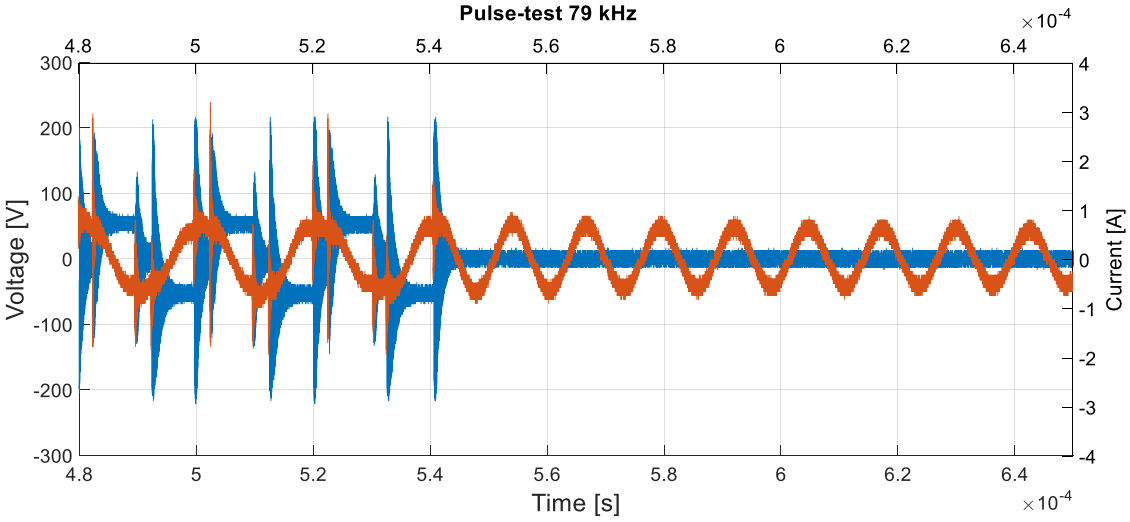

Figure 5.8 Pulse-test for the system 79 kHz with 50V

In comparison with figure 5.6, figure 5.8 shows a major difference between the current signal before and after the train of voltage pulses. Besides, due the higher voltage applied,

the resultant current and voltage peaks are also bigger. This features lead to recommend the use of lower voltages for the Pulse-test than the nominal voltage of the system (500 V).

It can be seen from figure 5.9, how the current's behaviour change when the resonance frequency of the system is further away from the Pulse-test frequency. Consequentially, the current peaks are wider and the current measure signal needs a little bit of time to stabilize itself.

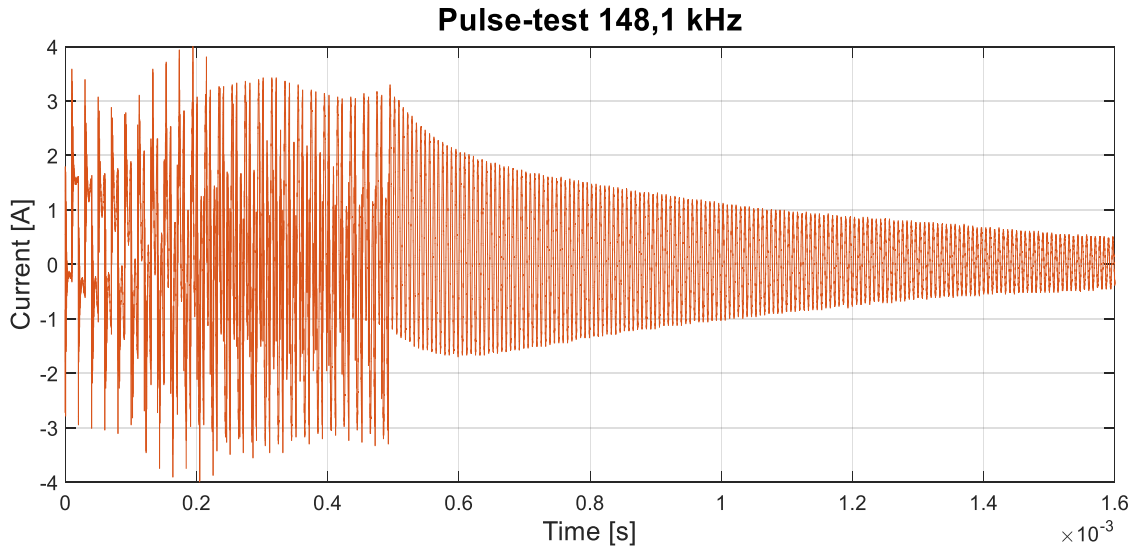

Figure 5.9 Current behaviour for the system 148,1 kHz under Pulse-test conditions

Finally, the Pulse-test has been tested with the Sensitec current sensors and the new developed measures ECU, which sends the zero crossing signal directly to the control ECU.

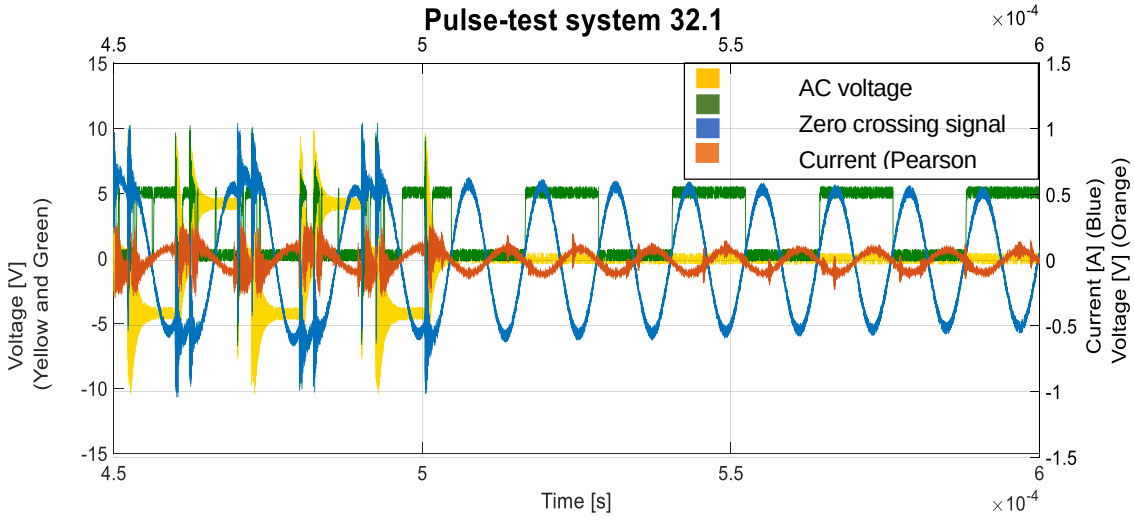

Figure 5.10 Pulse-test for system 32.1

After all the performed, tests two more conditions were established for the proper Pulse-test execution, which finally can be resumed as:

- Signal's frequency = 50 kHz
- Train of pulses length = 400 µs
- Acquisition time = 406 µs
- Voltage required = 30-50 V

5.3. PWM generation

The following figures show the obtained signals for the high side MOSFETs in both half-bridges when generating a PWM signal with D=0%, D=50% and D=100% respectively.

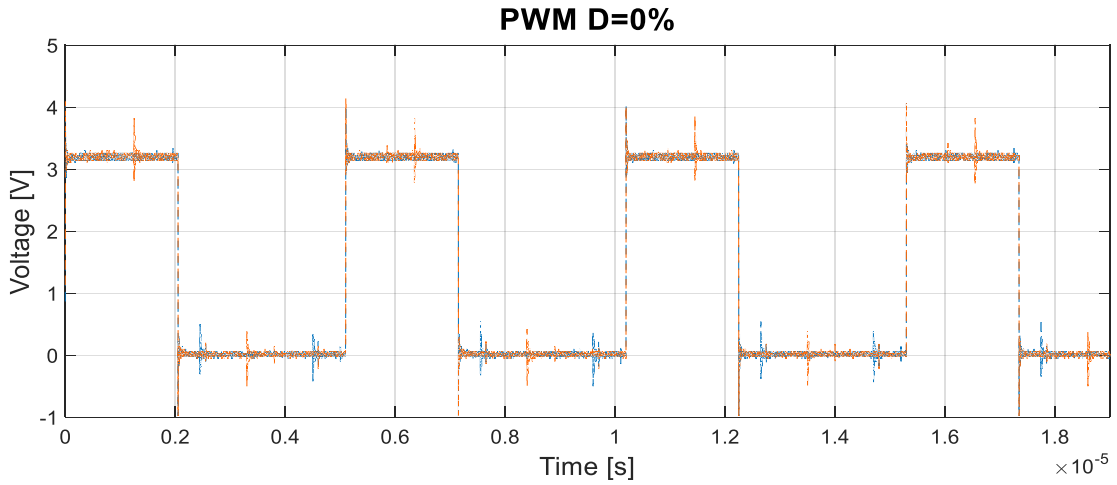

Figure 5.11PWM signal for D=0%

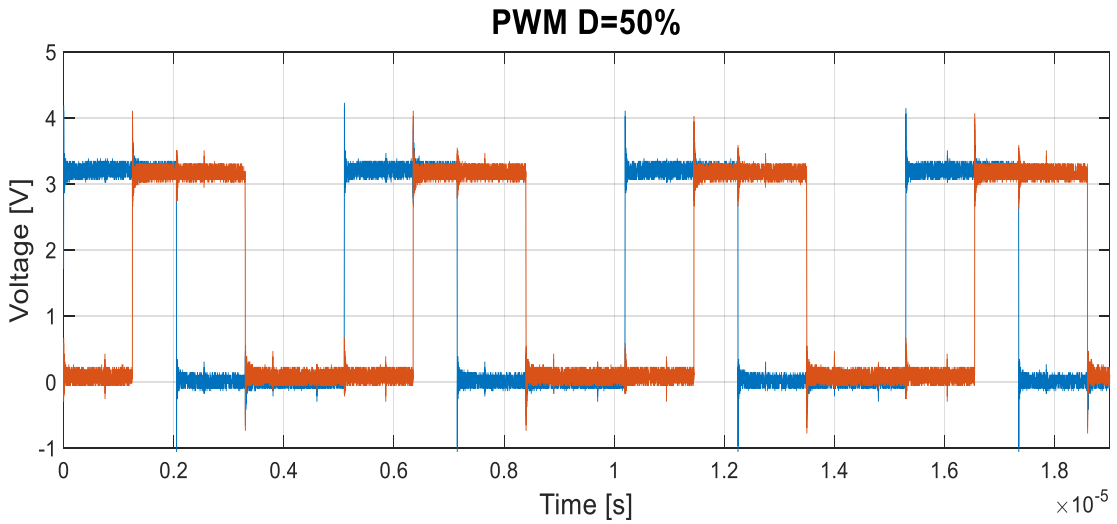

Figure 5.12 PWM signal for D=50%

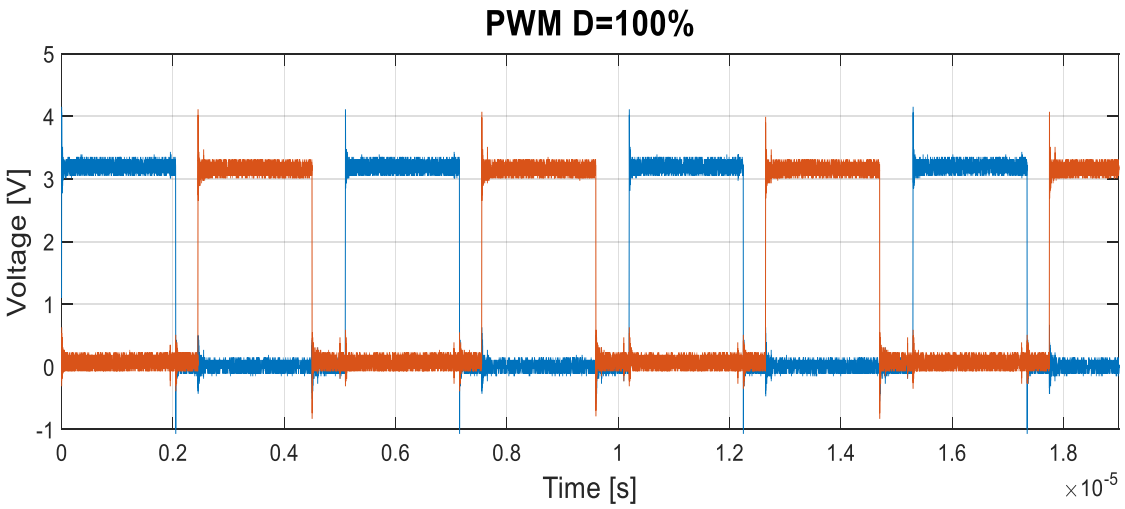

Figure 5.13 PWM signal for D=100%

5.4. Coupling factor measurement

Experimental measures have been taken in order to validate the model and simulations. One of the most important values to take into account is the coupling factor and to calculate it the process explained in [8] has been followed.

The figures 5.14 and 5.15 summarize the obtained results for both systems and a distance of 100 mm.

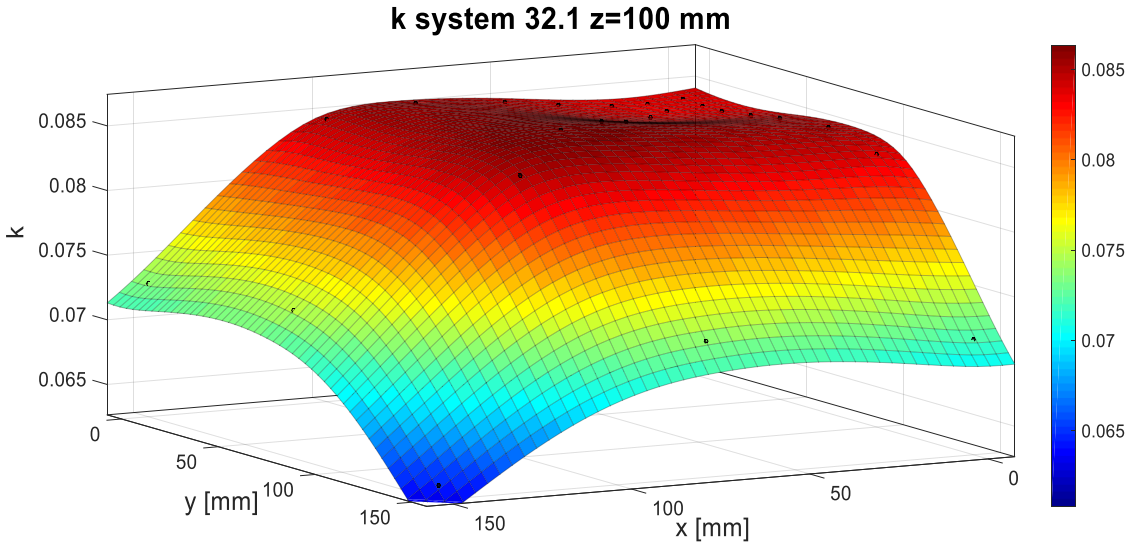

Figure 5.14 k for system 32.1 and z=100 mm

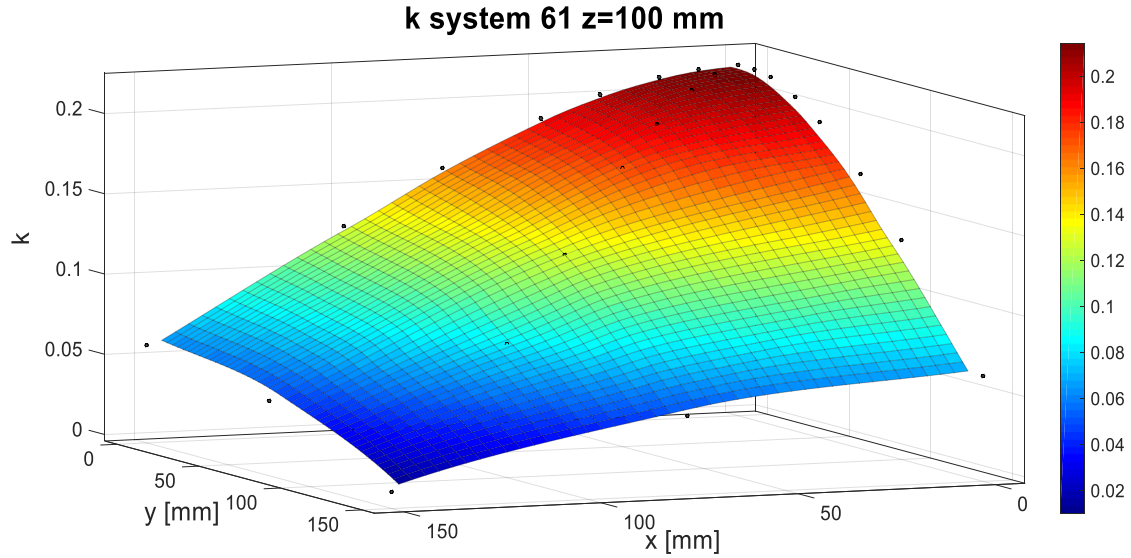

Figure 5.15 k for system 61 and z=100 mm

As can be seen in both pictures, each system agree with their expected behavior, the coupling factor of system 32.1 has a good offset behavior and it maintains almost plane for several distances, and the system 61 has in the nominal point a high coupling factor, but it sinks rapidly when distance increases.

Some differences were observed in comparison with the expected results. Some reasons regarding this error could be the geometry differences between the model and the real system. Besides, it could be possible that the metal frame used to perform the tests and the ground itself modify the inductance value of the windings.

5.5. Failure modes and effects analysis

As phase of the start-up process, it has been considered appropriate to study likely failures and possible malfunctions. Taken into account the worst case scenario gives an idea of the safety requirements and consequences that different problems could develop.

In this case, the study is oriented towards short-circuits and open load cases.

The several situations have been simulated using Simplorer, waiting 9 ms before the failure takes place. The table 5.1 summarizes the obtained results, all values are the resulting conditions after the failure.

Test	Short-circuit at L1	Short circuit at L2	Short circuit at Load	Open Load
I1 AC [A]	4000 (peaks)	500 rms	337 rms	170 rms
U L1 [V]	0	31100 rms	21213 rms	11000 rms
I L1 [A]	Decreasing	500 rms	337 rms	170 rms
U L2 [V]	0	0	6000 rms	713 rms
I L2 [A]	0	70 rms	268 rms	13 rms
U Load [V]	0	0	0	1000
I Load [A]	0	0	0	0
U C1 [V]	410 rms	0	21213 rms	10800 rms
IC1 [A]	4000 (peaks)	0	337 rms	170 rms
U C2 [V]	0	0	6000 rms	0
I C2 [A]	0	0	272 rms	0
Discharge time L1 [ms]	70	-	-	-

Table 5.1 Safety simulations summary

Can be extracted from the table that a short-circuit in the primary winding won't affect the secondary since no current will flow through L1 and consequently no magnetic field will be created.

All failure will lead to system's overload, but with the appropriate fuse in the primary winding the system will be free of damage. The selected fuse from the company Sitor, is rated at 160 A and is placed before the three phasic rectifier, splitting up the system from the grid.

As a complimentary information for the failure modes, in the figure 5.13 the discharging current through L1 in case of short circuit at this winding can be seen.

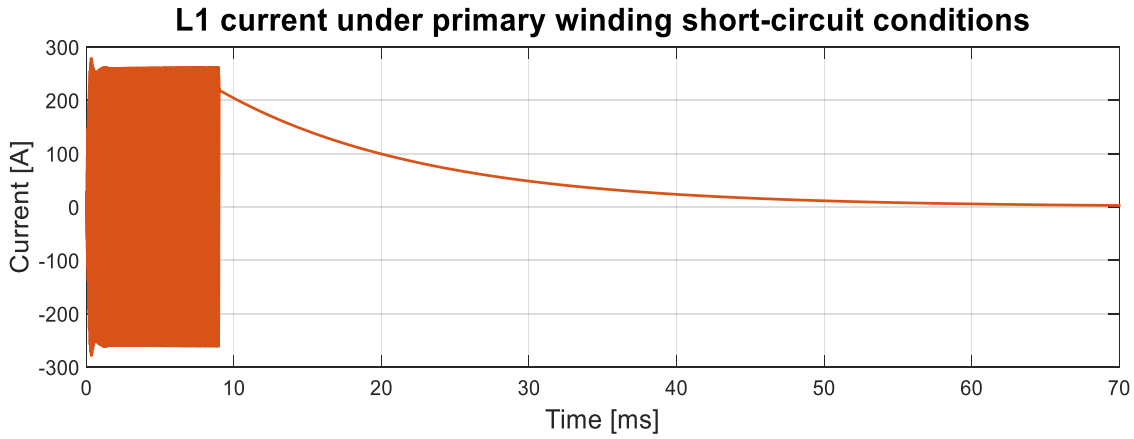

Figure 5.16 Current through L1 under short circuit conditions

5.6. System 32.1 Operation mode

In first place, the system has been characterized in order to know exactly the resonance frequency and the load nature in the frequency response. As can be seen in figure 5. , the resonance frequency it's about 83,8 kHz and if the frequency error is bigger than 1 kHz, the system will no longer operate under resonance frequency conditions, instead of that, will be working with a capacitive or an inductive load.

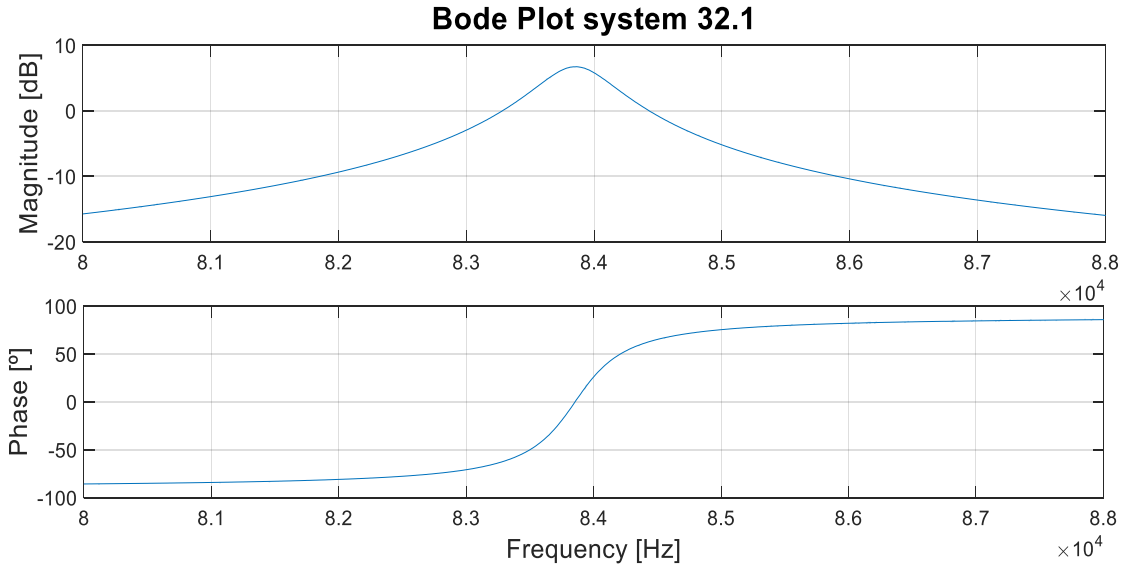

Figure 5.17 Bode plot system 32.1

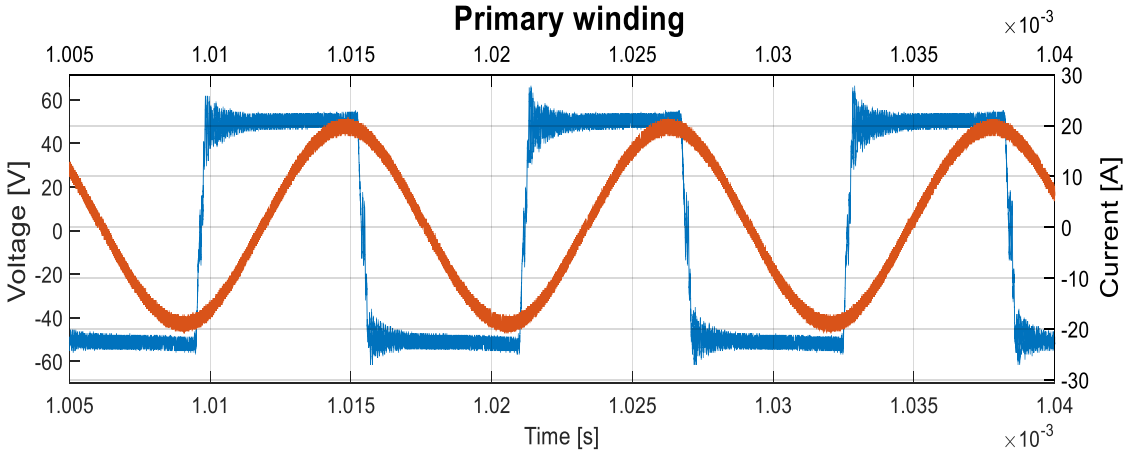

Figure 5.18 Primary winding's results for system 32.1

By the fact of testing the system with a power source of 1 kW, there were problems when trying to work near the frequency of resonance, because the current limitation of the power source was active and therefore, the voltage sank near to zero, like a short-circuit condition.

For this reason, can be seen in figure 5.18 how due working with a frequency greater than the resonance frequency of the system, the phase between voltage (blue) and current (orange) is 90º.

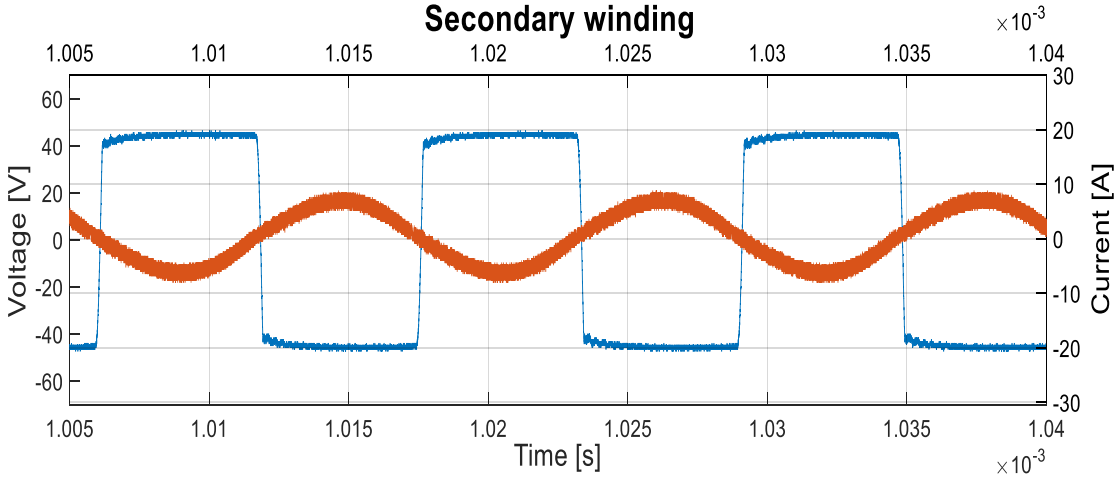

Figure 5.20 Secondary winding's results for system 32.1

On the other hand, on the secondary side, the phase between both signals is zero, due the resistive nature of the load. Furthermore, it can be seen that the voltage signal is also squared. This happens due the use of the secondary rectifier.

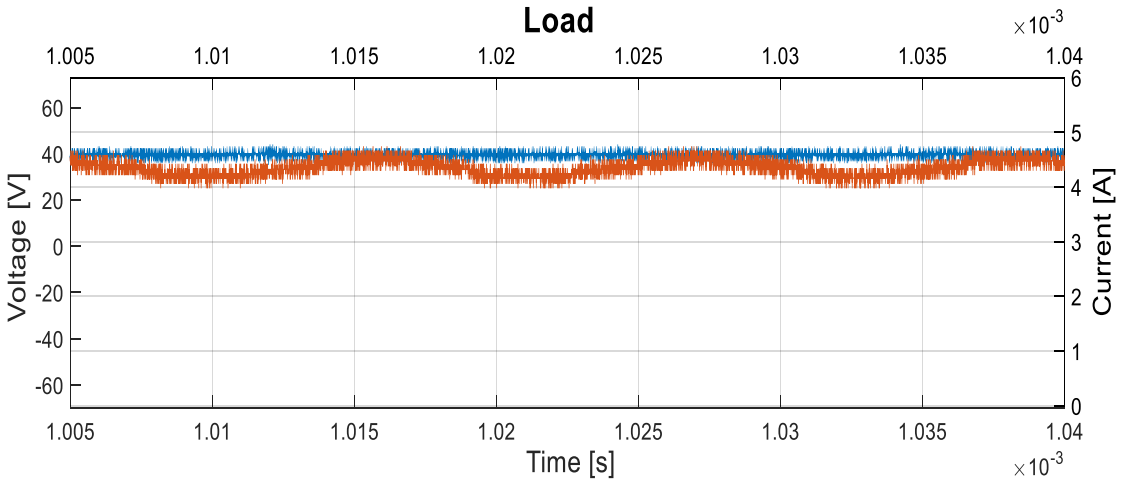

Figure 5.19 Load's results for system 32.1

The figure 5.20 shows the voltage and the current signals on the load, it can be observed that the voltage ripple is almost negligible and that the current ripple is about 0,5 A. The values of both ripples are considered acceptable for the use of charging and shows a good quality output for the battery charger.

5.7. System 61 Operation mode

The operating conditions for the system 61 are the same than the system 32.1 except for the frequency. The Bode plot for the system 61 shows that the resonance frequency is 70500 Hz, clearly different than the one expected from the simulations.

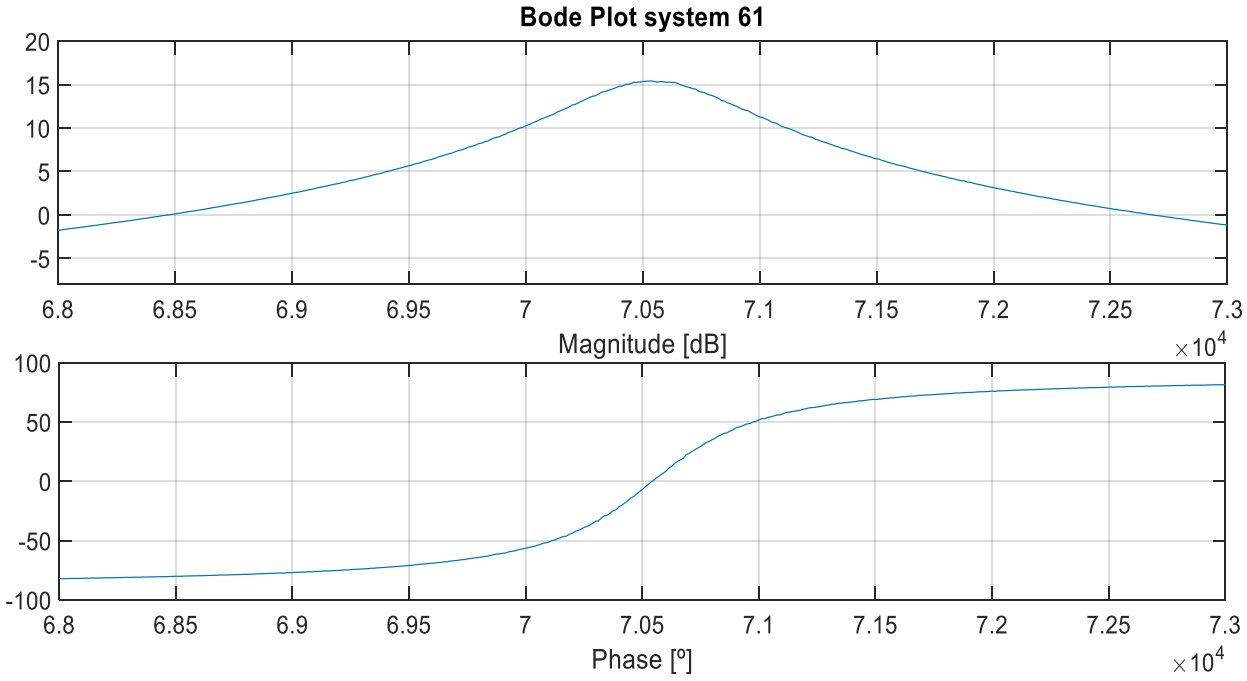

Figure 5.21 Bode plot system 61

Having a look at the results for the primary winding, it can be seen in figure 5.22, the results show that the load behaves as capacitive, that would mean that the resonance frequency would be higher than the used for the tests (81 kHz).

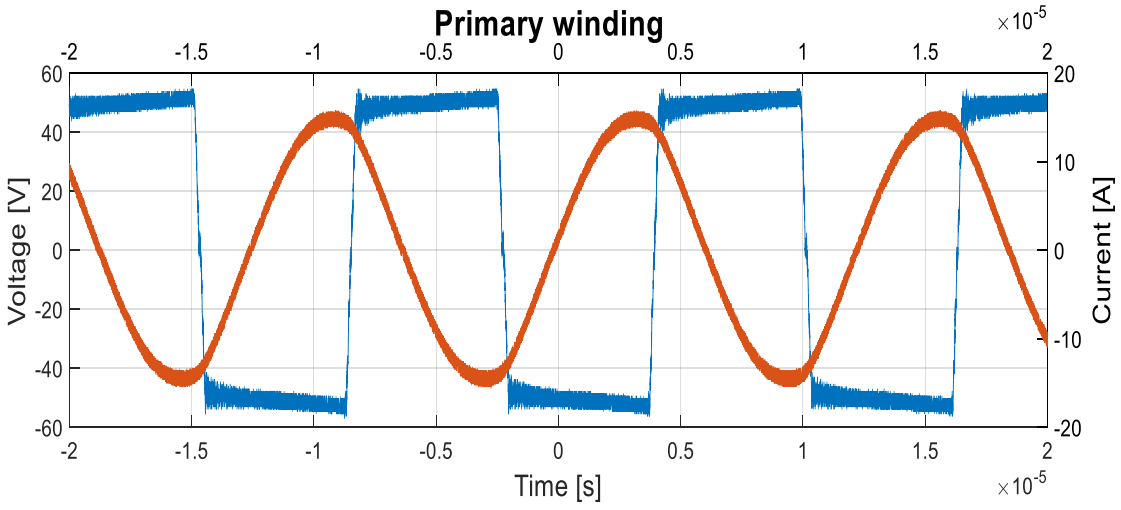

Figure 5.22 Primary winding's results for system 61

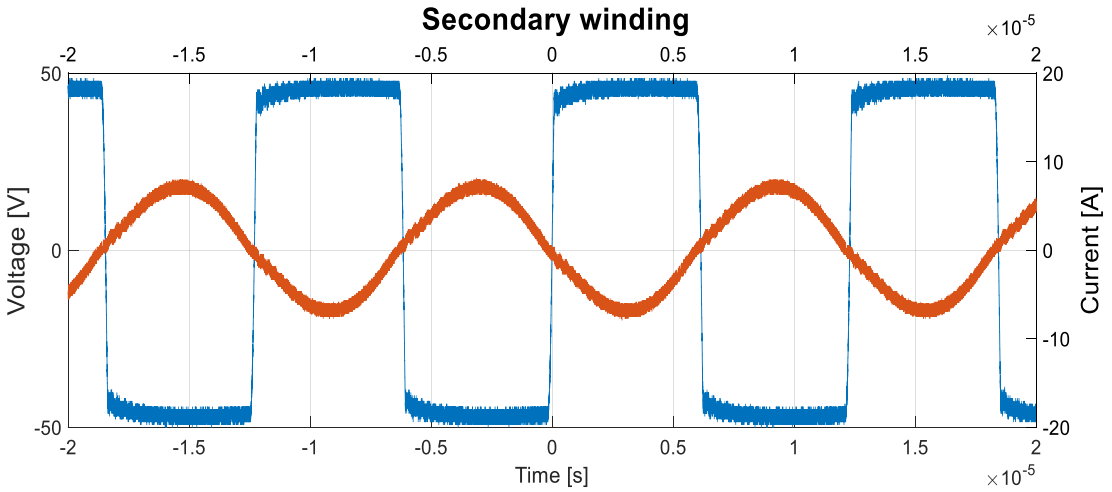

Figure 5.23 Secondary winding's results for system 61

The obtained results for the secondary side show the same behavior as the system 32.1, the voltage is squared and both signals have the same phase.

Finally, the figure 5.24 show the DC voltage and current obtained at the load. It can be observed how both signals have a very low ripple, being the voltage ripple almost negligible, and the current ripple of 0,5 A.

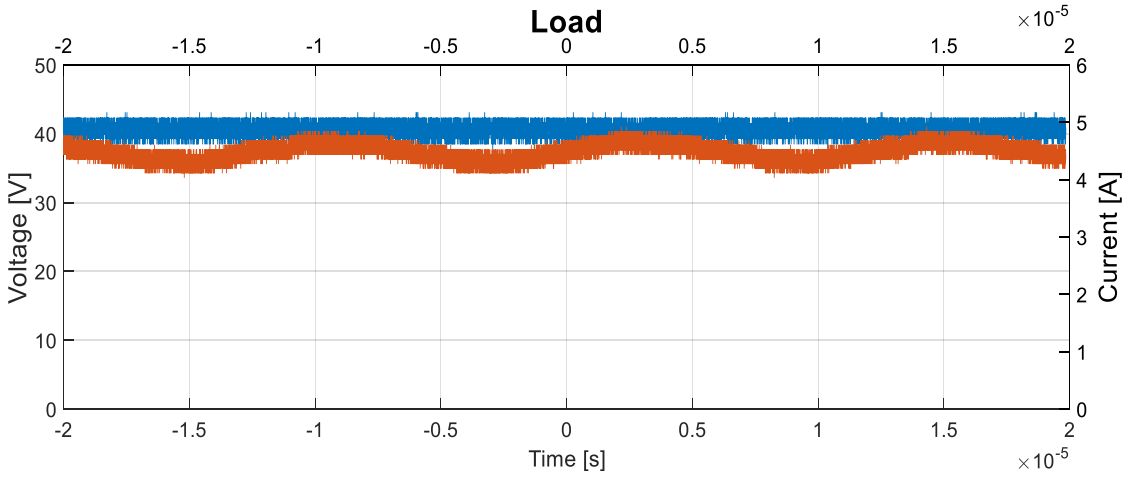

Figure 5.24 Load's results for system 61

The tables 5.2 and 5.3 summarize the performed tests for both system respectively with a duty cycle of 100% and an input voltage of 50 V. It can be seen that due the difference between the real resonance frequency and the theoretical, values as currents differ remarkably.

One interesting parameter to take into account is the global efficiency, obtaining an efficiency (from the power supply to the load of 0,87 for system 32.1 and an efficiency of 0,91 for the system 61.

Test	U1 AC rms [V]	I1 AC rms [A]	I1 DC [A]	U2 AC rms [V]	I2 AC rms [A]	U2 DC [V]	I2 DC [A]	η	φ (rad)	delta I2dc [A]
Real	50	13,5	4	44	4,65	40	4,35	0,87	1,5	0,5
Simulation	50	8,2	X	26	2,8	25	2,3		0,546	0,3

Table 5.2 Summary of the obtained results for system 32.1

Test	U1 AC rms [V]	I1 AC rms [A]	I1 DC [A]	U2 AC rms [V]	I2 AC rms [A]	U2 DC [V]	I2 DC [A]	η	φ (rad)	delta I2dc [A]
Real	50	9,81	4	45,2	4,78	40,5	4,5	0,91	1,5	0,5
Simulation	50	38,4	X	59,8	6,5	58,25	5,5		0,102	0,3

Table 5.3 Summary of the obtained results for system 61

6. Summary, conclusions and future work

The aim of this Master Thesis was to put all the knowledge, studies and work done in previous Master and Bachelor Thesis regarding inductive charging technology and finalizing the construction of those parts that were incomplete, being able to build the whole system and perform its start-up.

The done tasks include:

- Adjustment of the existing software to include failure detection of some critical parameters as temperature, current and voltage.
- Implementation of a software routine capable of recognize and calculate the resonance frequency of the system.
- Implementation of variable duty cycle and frequency PWM control for a full-bridge inverter.
- Design of a passive rectifier, involving PCB development, filter calculations, thermal studies, construction and testing.
- Measurement of the real coupling factor for both systems.
- Construction of the compensation modules, and compare the results with the theoretical simulations.
- Perform tests putting all the system together with both systems.
- Failure Modes and Effect Analysis

All required conditions are fulfilled, and the construction and start-up of both systems, successful.

The results show a clear difference between simulations and real tests, the reasons of these differences can be drawn from low accuracy in terms of signal frequency and the fact that the system can only change its frequency of commutation 1 kHz to 1 kHz. Besides, the system could only be tested using a voltage source of 1 kW, far from its maximal power of 44 kW.

Despite the possible differences between simulations and measurements, both systems present efficiencies near the target of 90%, demonstrating the good functioning of induction technology and it real application in case of battery charging for electric cars.

As further work to perform in a future, more tests need to be done to compare simulations and measurements. This tests should include high power testing to check its full operation conditioning.

Besides, it could be interesting to develop a second version of the control ECU, using a more powerful microcontroller, like a DSP. With a DSP the accuracy in terms of frequency of the signal generated would be better, and it will be possible to recognize higher frequencies for the pulse-test.

Other PWM controls could be studied in order to reduce the total harmonic distortion, generating a sinusoidal voltage signal.

Finally, it could be interesting to test the charger with a real battery, and also to develop a communication module prototype between the secondary winding + battery and the charger, simulating the real functioning as an electric car.

7. Appendix

7.1. Schematics and PCB layouts

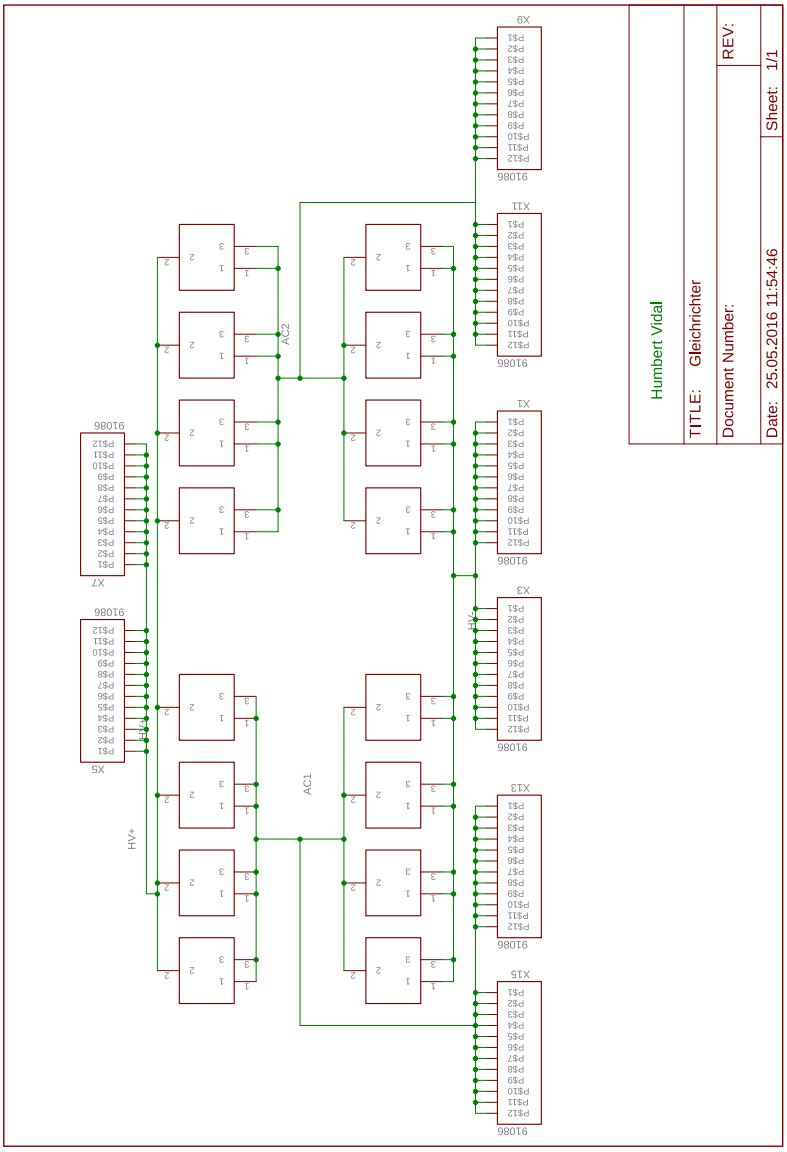

Figure 7.1 Rectifier's schematic

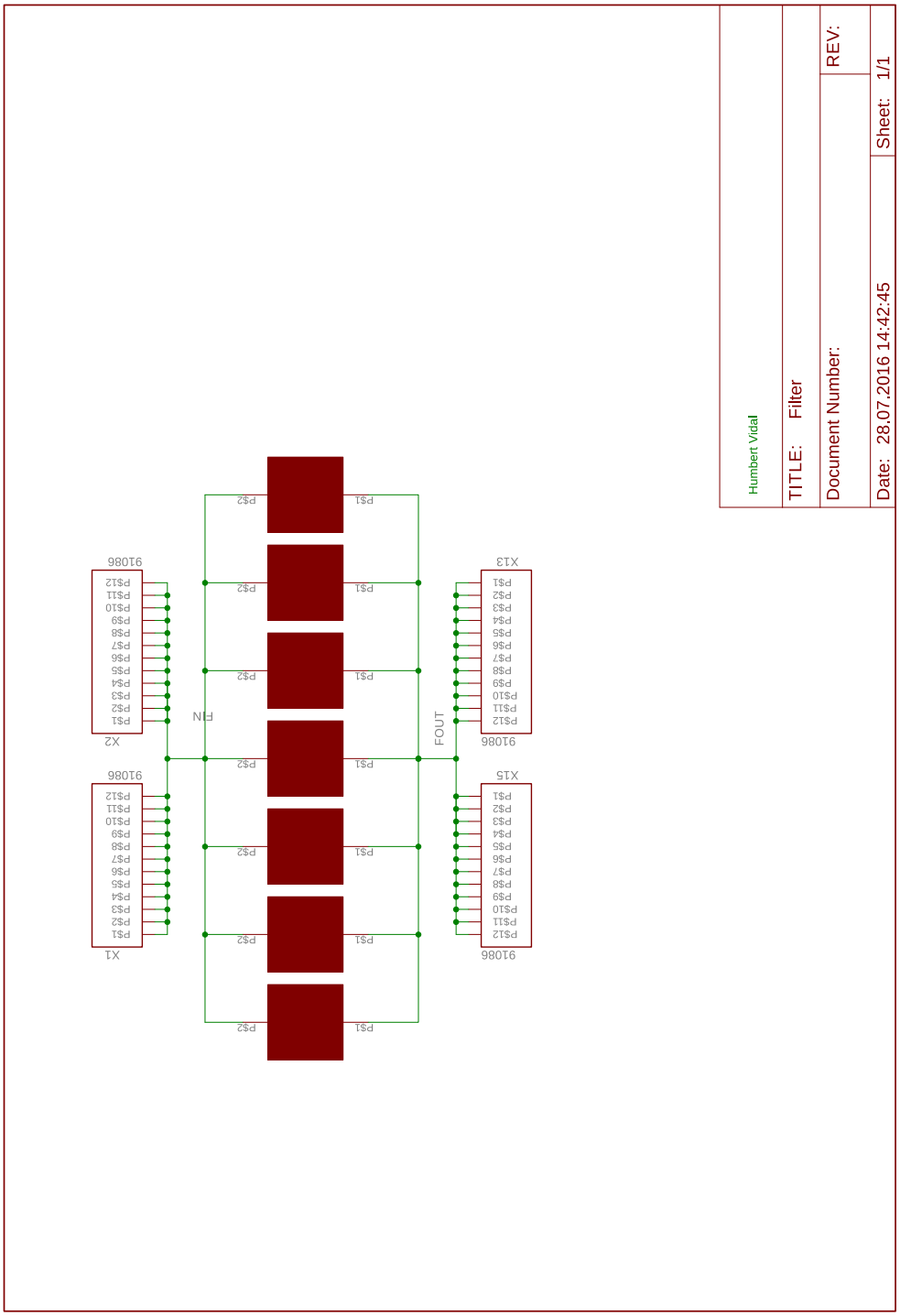

Figure 7.2 Filter's schematic

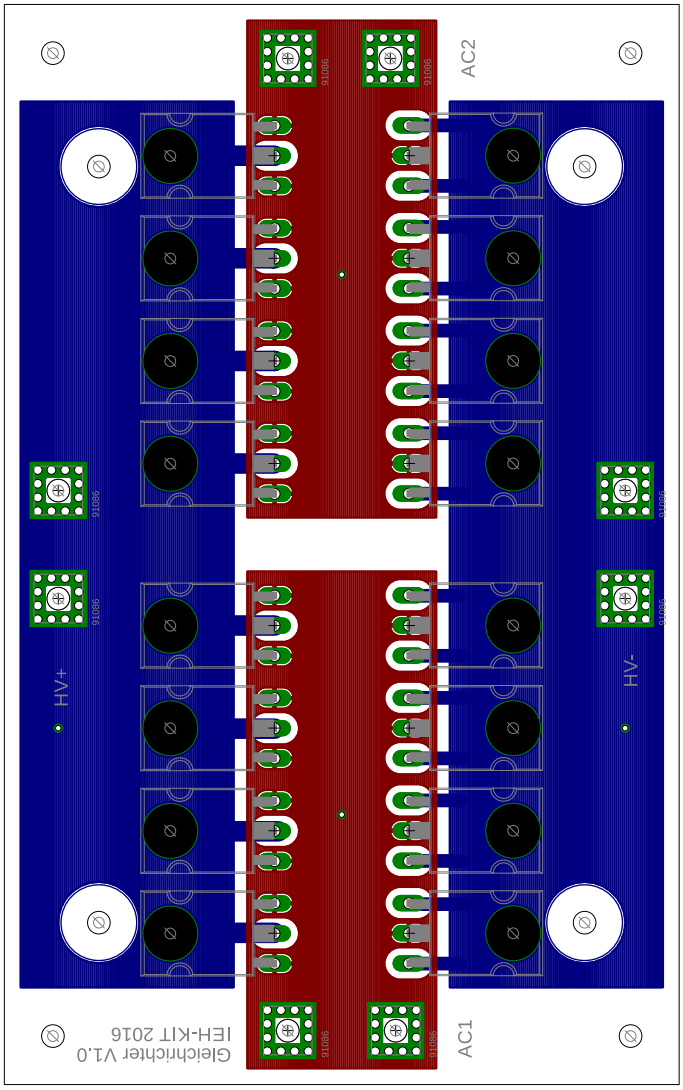

Figure 7.3 Rectifier's layout

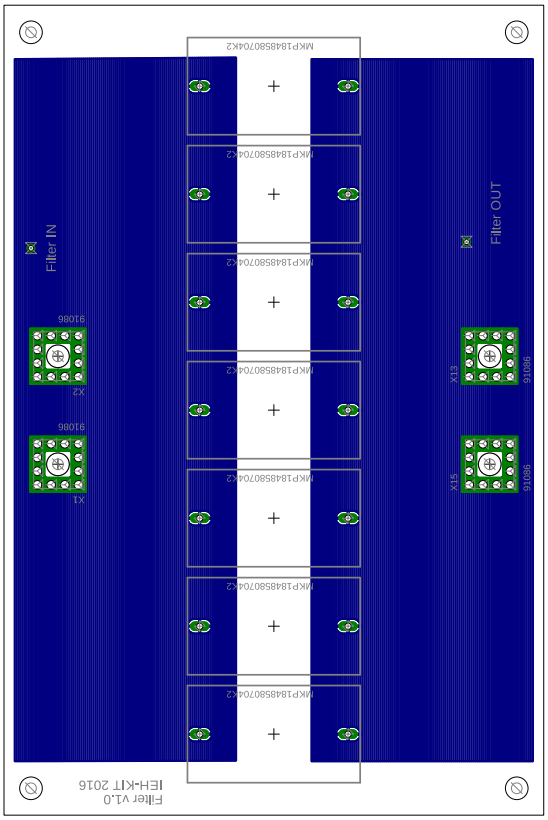

Figure 7.4 Filter's layout

7.2. Simplorer models

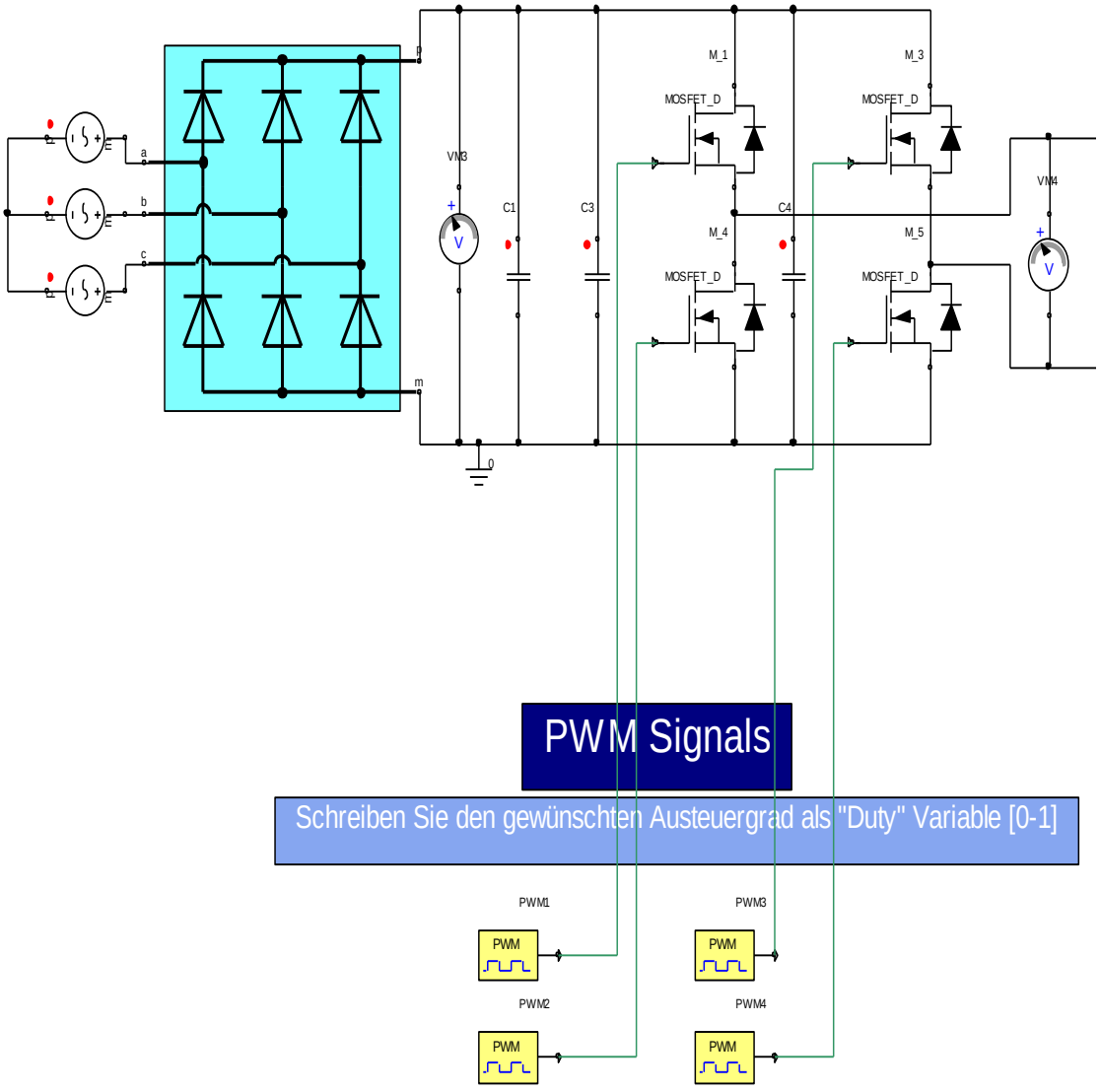

Figure 7.5 Grid, inverter and PWM control model

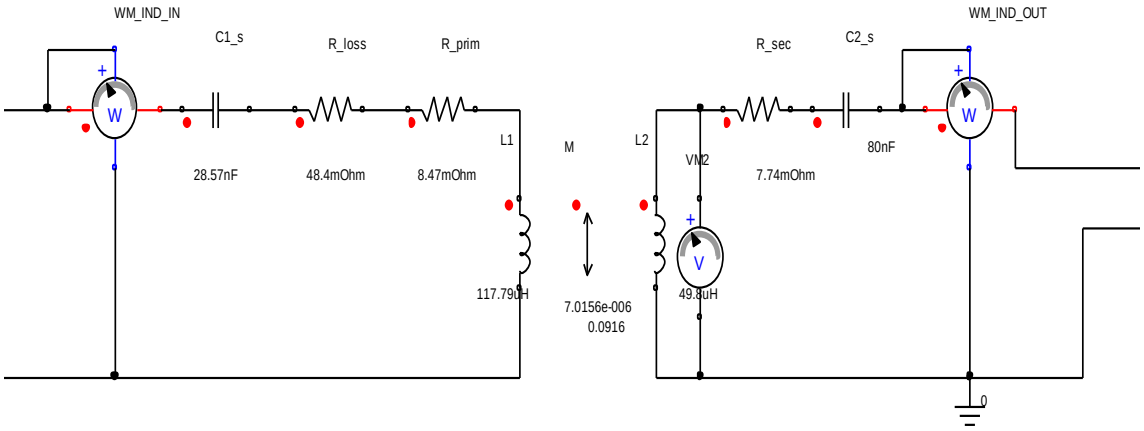

Figure 7.6 Primary and secondary winding and compensation model

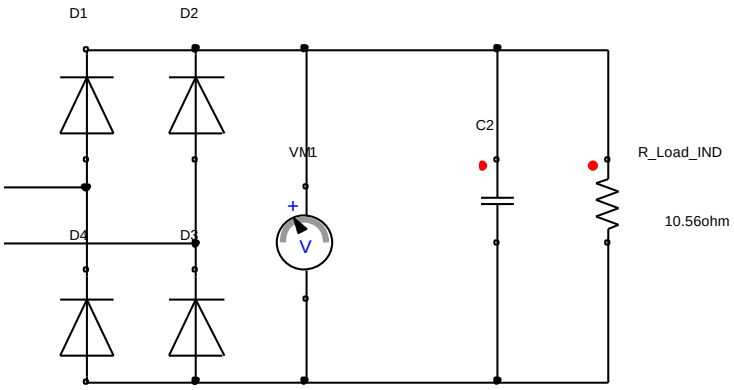

Figure 7.7 Secondary rectifier and filter model

7.3. Coupling coefficient measurements

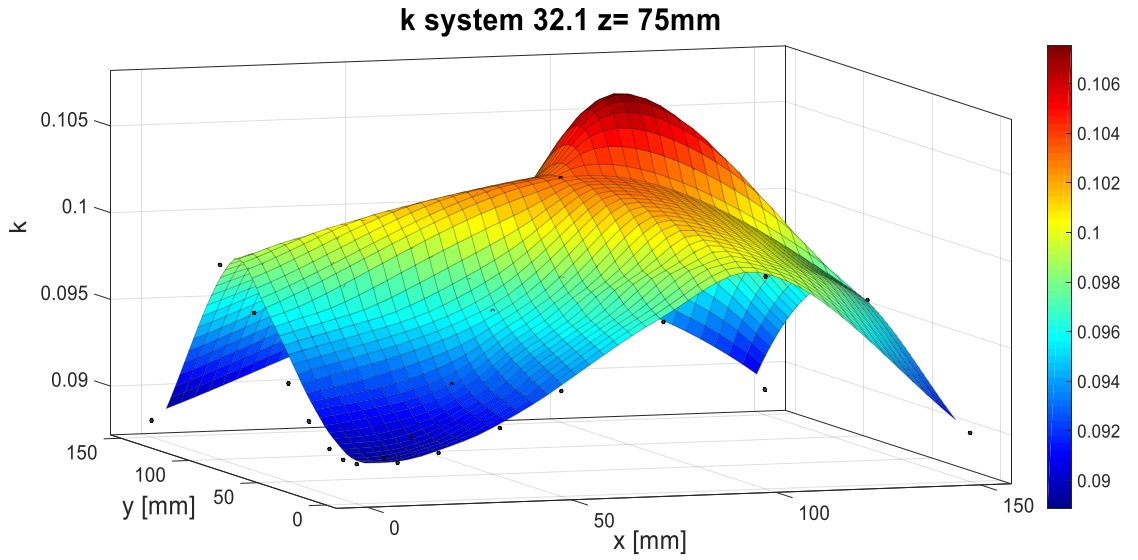

Figure 7.8 k for system 32. z=75mm

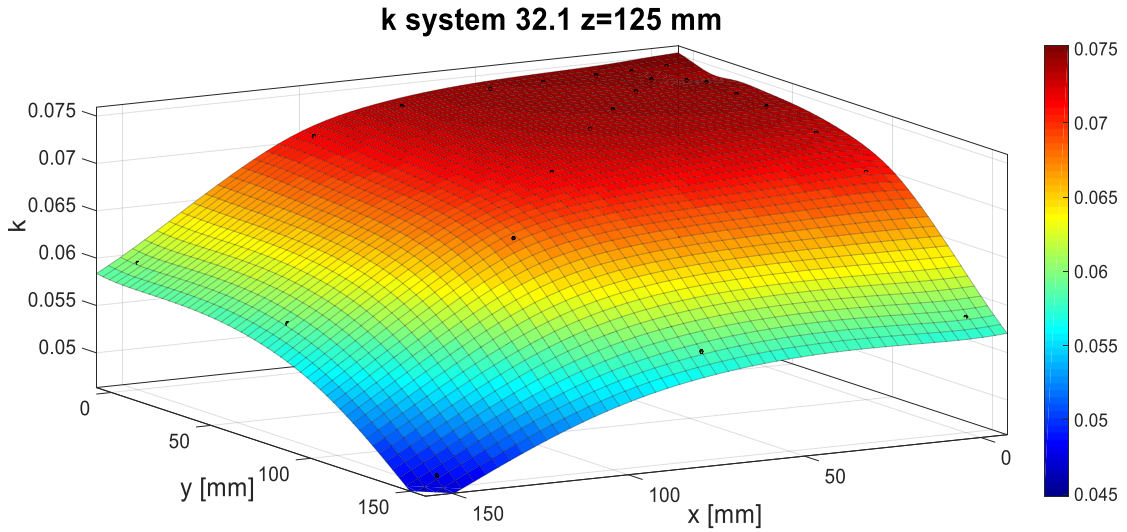

Figure 7.9 k for system 32.1 z=125mm

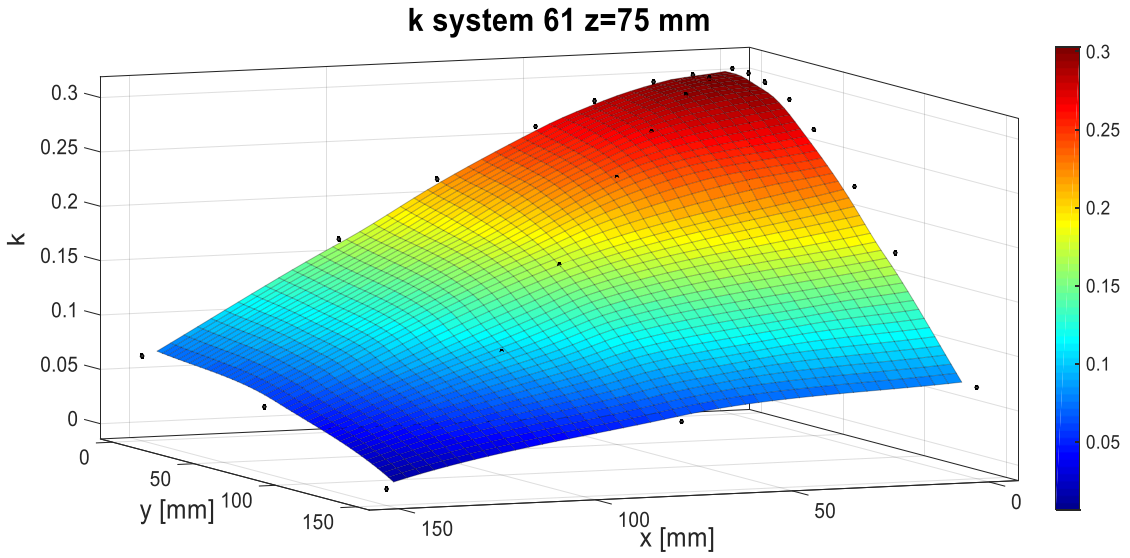

Figure 7.10 k for system 61 z =75mm

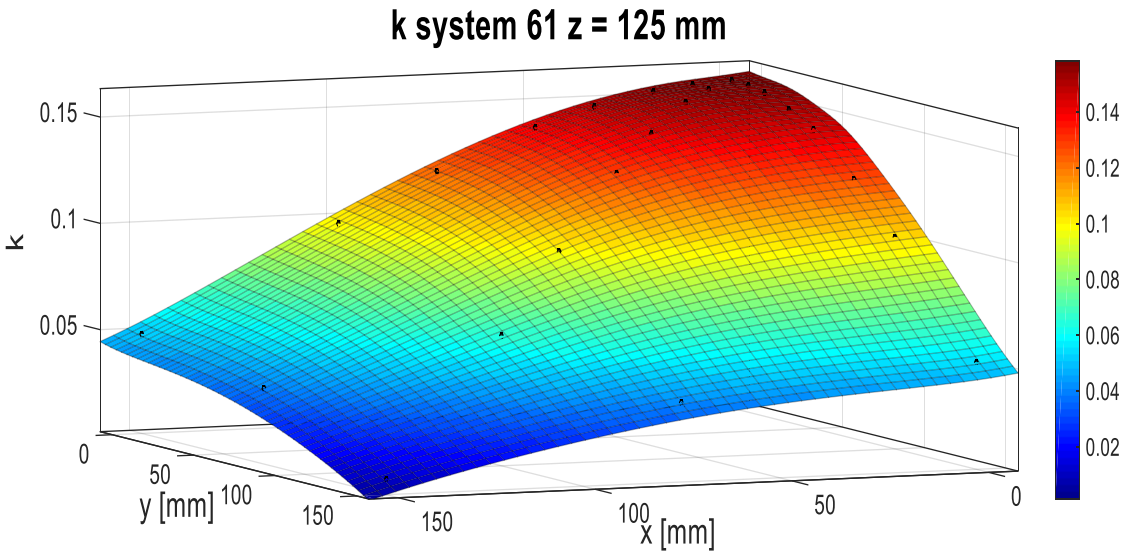

Figure 7.11 k for system 61 z=125mm

8. References

[1] **Bekker, Henk :** *„2015 (Full Year) Germany: Electric and hybrid car sales. (2016).* Available at: http://www.best-selling-cars.com/germany/2015-full-year-germany-electric-and-hybrid-car-sales.

[2] Image from: https://www.pluglesspower.com.

[3] **Mattsson, Petter ; Olsson, Kim :** *"High efficiency inductive charging for electric mini-cars" (Master thesis).* Chalmers University of Technology (2014).

[4] **Müller, Benedikt :** *"Entwicklung und Aufbau eines Rezonanzwandlers zum Betrieb induktiven Ladesysteme hoher Leistung im Themenfeld der Elektromobilität" (Master thesis).* Karlsruher Institut für Technologie (2015).

[5] **Sillman, Björn :** *"Entwurf und Aufbau eines Resonanzwandlers zur induktiven Energieübertragung" (Master thesis).* Karlsruher Institut für Technologie (2015).

[6] **Wolf, Manuel :** *"Entwicklung und Aufbau eines induktiven Energieübertragungssystems zur Untersuchung und Demonstration des kontaktlosen Ladens von Elektrofahrzeugen" (Master thesis).* Karlsruher Institut für Technologie (2015).

[7] Image from: https://www.maximintegrated.com/en/images/appnotes/726/726Fig02.gif

[8] **Lang, Benedikt :** *"Technise Vergleichanalyse zur Frequenznachführung beim kontaklosen Laden von Elektrofahrzeugen" (Bachelor thesis).* Karlsruher Institut für Technologie (2013).

[9] **Lörcher, Markus :** *" Entwicklung und Aufbau einer 3-Achsen-Positioniereinheit zur Vermessung experimenteler induktiver" (Bachelor thesis).* Karlsruher Institut für Technologie (2015).

[10] **Sudrià, Antoni ; Montesinos, Daniel:** "*Conversió de l'energia*" (2015) .

[11] Cree C3D16060D ,Datasheet, Cree Inc., 2013.

[12] Celem CSM 150 100 nF, Datasheet, Celem Power Capacitors, 2015.

[13] CMS 3100, Datasheet, Sensitec Gmbh, 2013.

[14] ATmega 324-P, Datasheet, Atmel Corporation, 2007.

[15] MKP1848, Datasheet, Vishay, 2016.